Prog. Theor. Exp. Phys. **2018**, 043B10 (24 pages)
DOI: 10.1093/ptep/pty042

Effective theory analysis for vector-like quark model

Takuya Morozumi[1,2], Yusuke Shimizu[1,*], Shunya Takahashi[1,*], and Hiroyuki Umeeda[3,*]

[1] *Core of Research for the Energetic Universe, Hiroshima University, Higashi-Hiroshima 739-8526, Japan*
[2] *Graduate School of Science, Hiroshima University, Higashi-Hiroshima 739-8526, Japan*
[3] *Graduate School of Science and Engineering, Shimane University, Matsue 690-8504, Japan*
*E-mail: yu-shimizu@hiroshima-u.ac.jp; s-takahashi@hiroshima-u.ac.jp; umeeda@riko.shimane-u.ac.jp

Received January 18, 2018; Revised March 13, 2018; Accepted March 16, 2018; Published April 27, 2018

We study a model with a down-type SU(2) singlet vector-like quark (VLQ) as a minimal extension of the standard model (SM). In this model, flavor-changing neutral currents (FCNCs) arise at tree level and the unitarity of the 3×3 Cabibbo–Kobayashi–Maskawa (CKM) matrix does not hold. In this paper, we constrain the FCNC coupling from $b \to s$ transitions, especially $B_s \to \mu^+\mu^-$ and $\bar{B} \to X_s\gamma$ processes. In order to analyze these processes we derive an effective Lagrangian that is valid below the electroweak symmetry breaking scale. For this purpose, we first integrate out the VLQ field and derive an effective theory by matching Wilson coefficients up to one-loop level. Using the effective theory, we construct the effective Lagrangian for $b \to s\gamma^{(*)}$. It includes the effects of the SM quarks and the violation of CKM unitarity. We show the constraints on the magnitude of the FCNC coupling and its phase by taking account of the current experimental data on ΔM_{B_s}, $\mathrm{Br}[B_s \to \mu^+\mu^-]$, $\mathrm{Br}[\bar{B} \to X_s\gamma]$, and CKM matrix elements, as well as theoretical uncertainties. We find that the constraint from $\mathrm{Br}[B_s \to \mu^+\mu^-]$ is more stringent than that from $\mathrm{Br}[\bar{B} \to X_s\gamma]$. We also obtain a bound for the mass of the VLQ and the strength of the Yukawa couplings related to the FCNC coupling of the $b \to s$ transition. Using the CKM elements that satisfy the above constraints, we show how the unitarity is violated on the complex plane.

Subject Index B40, B51, B52, B56

1. Introduction

After the discovery of the Glashow–Iliopoulos–Maiani mechanism [1], this suppression mechanism of the flavor-changing neutral current (FCNC) has been firmly verified in K, D, and B meson systems. The unitarity of the Cabibbo–Kobayashi–Maskawa (CKM) matrix [2–4] has also been verified. As investigated in Refs. [5,6], CKM unitarity is consistent with current data, which characterizes one of the most successful aspects in the standard model (SM).

As an extension of the quark sector, the vector-like quark (VLQ) is considered. Here, a VLQ is a quark whose representations in the gauge group for left- and right-handed components are the same. As models including VLQs, some new physics scenarios have been considered in the literature. Such vector-like extensions of the SM include the universal seesaw model [7–12]. This scenario introduces gauge singlet vector-like fermions to explain the hierarchical structure of fermion masses. Furthermore, in the context of left–right symmetry, the seesaw mechanism induced by vector-like fermions gives a solution to the strong CP problem [13].

The model with VLQ leads to rich phenomenology that can be testable in experiments [14–19]. In particular, FCNCs induced by VLQ give rise to deviation from the SM prediction. Furthermore, the

Funded by SCOAP^3

unitary relation of the CKM matrix, e.g. $V_{ub}^* V_{us} + V_{cb}^* V_{cs} + V_{tb}^* V_{ts} = 0$, no longer holds. The unitarity triangle is modified as a quadrilateral due to the correction that arises from FCNCs. On the other hand, the direct detection of the VLQ is under way in collider experiments [20,21]. Then, the predictions and constraints on the mass and couplings of VLQ from the flavor observables provide important information.

In this paper, a model including one additional down-type VLQ is discussed. Integrating out the VLQ, one can find that tree-level FCNC arises from interaction with the Z and Higgs bosons. On the basis of the effective field theory (EFT), we derive loop functions that correspond to the Inami–Lim functions in the SM. In order to examine the FCNC, phenomenological analysis is carried out for the $b \to s$ transition. Specifically, experimental data for $\bar{B} \to X_s \gamma$, $B_s \to \mu^+\mu^-$, and the mass difference in the B_s–$\bar{B}_s$ system are utilized to constrain the model. The constraints on the magnitude of the FCNC coupling and its phase are shown by taking account of the current experimental data as well as theoretical uncertainties.

This paper is organized as follows: In Sect. 2, we integrate out the down-type VLQ and determine the Wilson coefficients of the EFT up to one-loop level. The loop functions are summarized in Sect. 3. In Sect. 4, a phenomenological analysis for the $b \to s$ transition is given. Section 5 is devoted to summary and discussion.

2. Integrating out VLQ fields

In this section, we derive a low-energy effective Lagrangian by integrating out the VLQ fields. For this purpose, we show a full Lagrangian which includes one down-type SU(2) singlet VLQ in addition to the SM quarks. We assume that the mass of the VLQ is much larger than the electroweak (EW) scale. Then the Lagrangian $\mathcal{L}_{\rm Full}$ that is invariant under $\mathrm{SU(3)_c} \times \mathrm{SU(2)} \times \mathrm{U(1)_Y}$ is

$$\begin{aligned}\mathcal{L}_{\rm Full} = {} & \overline{q_L^i} i \not{D}_L q_L^i + \overline{u_R^i} i \not{D}_R^u u_R^i + \overline{d_R^i} i \not{D}_R^d d_R^i + \overline{d_L^4} i \not{D}_R^d d_L^4 + \overline{d_R^4} i \not{D}_R^d d_R^4 \\ & - [y_d^{ij} \overline{q_L^i} \phi d_R^j + y_d^{i4} \overline{q_L^i} \phi d_R^4 + M_4 \overline{d_L^4} d_R^4 + y_u^{ii} \overline{u_R^i} \tilde{\phi} q_L^i + \text{h.c.}],\end{aligned} \tag{1}$$

where $i = 1, 2, 3$ denotes the indices for generations, $d_{L,R}^4$ are VLQs, and y_u and y_d represent Yukawa couplings of up-type and down-type quarks respectively. The matrix for the Yukawa coupling of up-type quarks is taken to be real diagonal, while that of down-type quarks is a 3×4 matrix. M_4 denotes the mass of the VLQ. Note that the mixing term between the left-handed VLQ d_L^4 and right-handed SM down-type quarks d_R^i is allowed in general. However, we can remove the mixing term by rotation of the down-type quarks. Hence we can take the Lagrangian as Eq. (1). The covariant derivatives are defined as follows:

$$D_{L\mu} = \partial_\mu + i g_s \frac{\lambda^a}{2} G_\mu^a + i g \frac{\tau^I}{2} W_\mu^I + i g' \frac{Y_{qL}}{2} B_\mu, \tag{2}$$

$$D_{R\mu}^u = \partial_\mu + i g_s \frac{\lambda^a}{2} G_\mu^a + i g' \frac{Y_{uR}}{2} B_\mu, \tag{3}$$

$$D_{R\mu}^d = \partial_\mu + i g_s \frac{\lambda^a}{2} G_\mu^a + i g' \frac{Y_{dR}}{2} B_\mu, \tag{4}$$

where λ^a, τ^I, and Y_X are Gell-Mann matrices, Pauli matrices, and the $\mathrm{U(1)_Y}$ hypercharge of a field X ($X = q_L, u_R, d_R$), respectively.

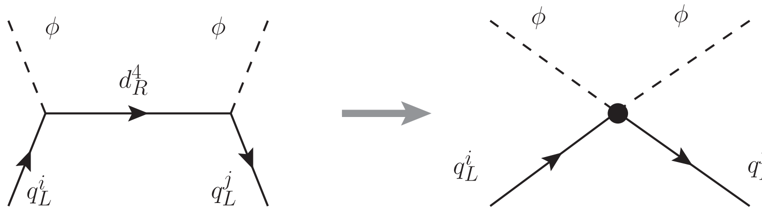

Fig. 1. The Feynman diagrams for the scattering of a quark / anti-quark pair into a Higgs pair ($q^i\overline{q}^j \to \phi\phi^\dagger$). The left figure shows the diagram of the full theory in which the VLQ is exchanged, while the right figure shows the diagram of the effective theory where the VLQ is absent and already integrated out.

2.1. *Matching full theory and effective theory*

In order to obtain the higher-dimensional operators that represent the effect of the VLQ in the energy scale between M_4 and the EW scale, we integrate out the VLQ fields $d^4_{L,R}$ in Eq. (1). At first, we perform tree-level matching at VLQ mass scale M_4. In Fig. 1, we show the Feynman diagram (left figure) for the scattering of a quark / anti-quark pair into a Higgs pair ($q^i\overline{q}^j \to \phi\phi^\dagger$), in which the VLQ is exchanged. We assume that the external particles have momenta much smaller than the mass of the VLQ. Then the amplitude of the left figure can be reproduced up to $\mathcal{O}(M_4^{-2})$ accuracy by computing the Feynman diagram of the right figure with the following low-energy effective Lagrangian [18,19,22–24]:

$$\mathcal{L}^{\text{tree}}_{\text{Eff}} = i\frac{y_d^{j4}y_d^{i4*}}{M_4^2}\left(\overline{q_L^j}\phi\right)\not{D}_R^d\left(\phi^\dagger q_L^i\right), \tag{5}$$

where $i, j = 1, 2, 3$.

The effective Lagrangian is written in terms of a dimension-six operator, and its coefficient is determined so that it reproduces the amplitude of the left figure in Fig. 1 within the precision of $\mathcal{O}(M_4^{-2})$. By using the equations of motion derived from the SM Lagrangian, we can rewrite the effective Lagrangian of Eq. (5):

$$\begin{aligned}\mathcal{L}^{\text{tree}}_{\text{Eff}} = \frac{y_d^{j4}y_d^{i4*}}{2M_4^2}\Bigg[&\frac{i}{2}\left(\overline{q_L^j}\tau^I\gamma^\mu q_L^i\right)\left\{\left(D_\mu\phi\right)^\dagger\tau^I\phi - \phi^\dagger\tau^I\left(D_\mu\phi\right)\right\}\\
&+\frac{i}{2}\left(\overline{q_L^j}\gamma^\mu q_L^i\right)\left\{\left(D_\mu\phi\right)^\dagger\phi - \phi^\dagger\left(D_\mu\phi\right)\right\}\\
&+\left(\phi^\dagger\phi\right)\left(y_d^{ik}\overline{q_L^j}\phi d_R^k + y_d^{jk*}\overline{d_R^k}\phi^\dagger q_L^i\right)\\
&+\frac{1}{2}\left(\phi^\dagger\tau^I\phi\right)\left\{y_u^{ij}\left(\overline{q_L^j}\tau^I\tilde{\phi}\right)u_R^j + y_u^{ij*}\overline{u_R^j}\left(\tilde{\phi}^\dagger\tau^I q_L^j\right)\right\}\\
&+\frac{1}{2}\left(\phi^\dagger\phi\right)\left\{y_u^{jj}\overline{q_L^j}\tilde{\phi}u_R^j + y_u^{jj*}\overline{u_R^j}\tilde{\phi}^\dagger q_L^j\right\}\Bigg].\end{aligned} \tag{6}$$

Next we consider one-loop level matching between the full theory and the effective theory to obtain effective interactions that contribute to the radiative transition of the quarks. The procedure is as follows:

(i) We calculate the amplitudes of the Feynman diagrams for the decay of q_L^i into q_L^j and one of the gauge fields B, W^I, or G^a at one-loop level (see the top figures in Fig. 2). These diagrams

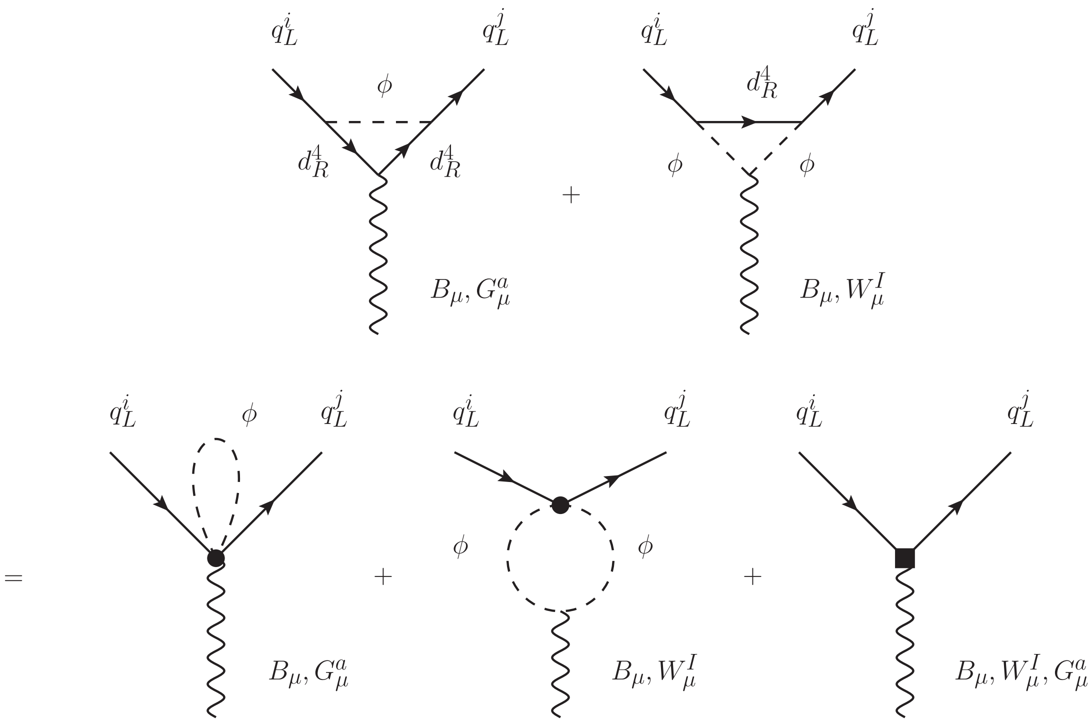

Fig. 2. The Feynman diagrams for the decay of q_L^i into q_L^j and one of the gauge fields B, W^I, or G^a at one-loop level with the full theory (top figures) and the effective theory (bottom-left and bottom-center figures). The circular marks denote the tree-level effective operator and the square mark denotes the new effective operators.

include the VLQ in the internal line. In this calculation, we renormalize the amplitudes with the $\overline{\text{MS}}$ scheme.

(ii) We calculate the same transitions as those of step (i) with the effective operator in Eq. (5) obtained by tree-level matching (see the bottom-left and bottom-center figures in Fig. 2). In this calculation, we also renormalize the amplitudes with the $\overline{\text{MS}}$ scheme.

(iii) We introduce new effective operators and determine their coefficients so that the renormalized amplitudes in step (ii) match with those of the full theory computed in step (i)—see the bottom-right figure in Fig. 2.

We can obtain the following effective Lagrangian $\mathcal{L}_{\text{Eff}}^{\text{one-loop}}$ at one-loop level:

$$\mathcal{L}_{\text{Eff}}^{\text{one-loop}} = \mathcal{L}_{\text{Eff}}^{K} + \mathcal{L}_{\text{Eff}}^{B} + \mathcal{L}_{\text{Eff}}^{W} + \mathcal{L}_{\text{Eff}}^{G}, \tag{7}$$

where

$$\begin{aligned}\mathcal{L}_{\text{Eff}}^{K} &= i\frac{y_d^{j4} y_d^{i4*}}{16\pi^2}\left(\frac{1}{2}\ln\frac{\mu^2}{M_4^2} + \frac{3}{4}\right)\overline{q_L^j}\mathbb{D}_L q_L^i \\ &\quad + i\frac{1}{16\pi^2}\frac{y_d^{j4} y_d^{i4*}}{3M_4^2}\left(y_d^{jl*}\overline{d_R^l}\phi^\dagger + y_u^{jj*}\overline{u_R^j}\tilde{\phi}^\dagger\right)\mathbb{D}_L\left(y_d^{ik}\phi d_R^k + y_u^{ii}\tilde{\phi}u_R^i\right),\end{aligned} \tag{8}$$

$$\mathcal{L}^{B}_{\mathrm{Eff}} = g'^2 \frac{y_d^{j4} y_d^{i4*}}{16\pi^2 M_4^2} \left\{ \frac{Y_{dR}}{2} \cdot \frac{7}{36} - \frac{Y_\phi}{2} \left(\frac{1}{6} \ln \frac{\mu^2}{M_4^2} + \frac{11}{36} \right) \right\}$$
$$\times \left(\overline{q_L^j} \gamma^\mu q_L^i \right) \left[\frac{Y_{lL}}{2} \overline{l_L} \gamma_\mu l_L + \frac{Y_{eR}}{2} \overline{e_R} \gamma_\mu e_R + \frac{Y_{qL}}{2} \overline{q_L} \gamma_\mu q_L + \frac{Y_{uR}}{2} \overline{u_R} \gamma_\mu u_R \right.$$
$$\left. + \frac{Y_{dR}}{2} \overline{d_R} \gamma_\mu d_R + i \frac{Y_\phi}{2} \left\{ \phi^\dagger D_\mu \phi - (D_\mu \phi)^\dagger \phi \right\} \right]$$
$$+ g' \frac{1}{16\pi^2 M_4^2} \left(\frac{Y_{qL}}{2} \cdot \frac{1}{12} - \frac{Y_{dR}}{2} \cdot \frac{1}{8} \right) \left[y_d^{j4} y_d^{i4*} \overline{q_L^j} \sigma_{\mu\nu} \left(y_d^{il} \phi d_R^l + y_u^{ii} \tilde{\phi} u_R^i \right) B^{\mu\nu} + \text{h.c.} \right], \quad (9)$$

$$\mathcal{L}^{W}_{\mathrm{Eff}} = -g^2 \frac{y_d^{j4} y_d^{i4*}}{16\pi^2 M_4^2} \left(\frac{1}{6} \ln \frac{\mu^2}{M_4^2} + \frac{11}{36} \right) \overline{q_L^j} \gamma^\mu \frac{\tau^I}{2} q_L^i$$
$$\times \left[\overline{l_L} \frac{\tau^I}{2} \gamma_\mu l_L + \overline{q_L} \frac{\tau^I}{2} \gamma_\mu q_L + i \left\{ \phi^\dagger \frac{\tau^I}{2} D_\mu \phi - (D_\mu \phi)^\dagger \frac{\tau^I}{2} \phi \right\} \right]$$
$$+ g \frac{1}{16\pi^2 M_4^2} \cdot \frac{1}{12} \left\{ y_d^{j4} y_d^{i4*} \overline{q_L^j} \frac{\tau^I}{2} \sigma_{\mu\nu} \left(y_d^{il} \phi d_R^l + y_u^{ii} \tilde{\phi} u_R^i \right) W^{I\mu\nu} + \text{h.c.} \right\}, \quad (10)$$

$$\mathcal{L}^{G}_{\mathrm{Eff}} = g_s^2 \frac{y_d^{j4} y_d^{i4*}}{16\pi^2 M_4^2} \cdot \frac{7}{36} \left(\overline{q_L^j} \gamma^\mu \frac{\lambda^a}{2} q_L^i \right) \left(\overline{q_L} \frac{\lambda^a}{2} \gamma_\mu q_L + \overline{u_R} \frac{\lambda^a}{2} \gamma_\mu u_R + \overline{d_R} \frac{\lambda^a}{2} \gamma_\mu d_R \right)$$
$$+ g_s \frac{1}{16\pi^2 M_4^2} \left(-\frac{1}{24} \right) \left\{ y_d^{j4} y_d^{i4*} \overline{q_L^j} \frac{\lambda^a}{2} \sigma_{\mu\nu} \left(y_d^{il} \phi d_R^l + y_u^{ii} \tilde{\phi} u_R^i \right) G^{a\mu\nu} + \text{h.c.} \right\}. \quad (11)$$

To derive the above expressions, we use the equation of motion in the leading order of the expansion with respect to $1/M_4^2$, namely that of the SM. In Eqs. (9)–(11), $F_B^{\mu\nu}$, $W^{I\mu\nu}$, and $G^{a\mu\nu}$ are the field strength of $\mathrm{U(1)_Y}$, SU(2), and $\mathrm{SU(3)_c}$, respectively. The matching scale μ is typically taken to be the VLQ mass scale M_4. The lepton doublet is denoted by l_L. The effective Lagrangians $\mathcal{L}^B_{\mathrm{Eff}}$, $\mathcal{L}^W_{\mathrm{Eff}}$, and $\mathcal{L}^G_{\mathrm{Eff}}$ contain the effective operators that contribute to the decay of $q_L^i \to q_L^j B$, W^I, and G^a, respectively. Since we use the equations of motion, the effective Lagrangians also contain the operators such as the four-Fermi operators that do not contribute to these processes.

Finally, the whole Lagrangian $\mathcal{L}_{\mathrm{Eff}}$ obtained by integrating out the VLQ fields is given as:

$$\mathcal{L}_{\mathrm{Eff}} = \mathcal{L}_{\mathrm{SM}} + \mathcal{L}^{\mathrm{tree}}_{\mathrm{Eff}} + \mathcal{L}^{\mathrm{one-loop}}_{\mathrm{Eff}}, \quad (12)$$
$$\mathcal{L}_{\mathrm{SM}} = \overline{q_L^i} i \not{D}_L q_L^i + \overline{u_R^i} i \not{D}_R^u u_R^i + \overline{d_R^i} i \not{D}_R^d d_R^i - [y_d^{ij} \overline{q_L^i} \phi d_R^j + y_u^{ii} \overline{u_R^i} \tilde{\phi} q_L^i + \text{h.c.}], \quad (13)$$

where $\mathcal{L}^{\mathrm{tree}}_{\mathrm{Eff}}$ is given in Eq. (5) or Eq. (6), and $\mathcal{L}^{\mathrm{one-loop}}_{\mathrm{Eff}}$ is given in Eqs. (8)–(11). In Eq. (12), the kinetic term of the SM quark doublet q_L is

$$\mathcal{L}^q_{\mathrm{K}} = \overline{q_L^j} \left\{ \delta^{ji} + Z^{ji}(\mu) \right\} i \not{D}_L q_L^i, \quad (14)$$

$$Z^{ji}(\mu) = \frac{y_d^{j4} y_d^{i4*}}{16\pi^2} \left(\frac{1}{2} \ln \frac{\mu^2}{M_4^2} + \frac{3}{4} \right), \quad (15)$$

where the term $Z^{ji}(\mu)$ comes from the first term in Eq. (8). To rewrite the kinetic term into a canonical form, we perform the following rescaling of q_L:

$$q_L'^k \equiv \left\{\delta^{ki} + \frac{1}{2}Z^{ki}(\mu)\right\} q_L^i. \tag{16}$$

Then the kinetic term of the quark doublet becomes

$$\mathcal{L}_{\mathrm{K}}^q = \overline{q_L'^k} i\not{D}_L q_L'^k. \tag{17}$$

In terms of the rescaled fields introduced in Eq. (16), the Yukawa interactions in Eq. (13) are changed:

$$y_u^{ii}\overline{q_L^i}\tilde{\phi}u_R^i = \left\{\delta^{ki} - \frac{1}{2}Z^{ki}(\mu)\right\} y_u^{ii}\overline{q_L'^k}\tilde{\phi}u_R^i \equiv Y_u^{ki}\overline{q_L'^k}\tilde{\phi}u_R^i, \tag{18}$$

$$y_d^{ji}\overline{q_L^j}\phi d_R^i = \left\{\delta^{kj} - \frac{1}{2}Z^{kj}(\mu)\right\} y_d^{ji}\overline{q_L'^k}\phi d_R^i \equiv Y_d^{ki}\overline{q_L'^k}\phi d_R^i, \tag{19}$$

where we redefine the SM Yukawa coupling as

$$Y_u^{ki} \equiv \left\{\delta^{ki} - \frac{1}{2}Z^{ki}(\mu)\right\} y_u^{ii}, \quad Y_d^{ki} \equiv \left\{\delta^{kj} - \frac{1}{2}Z^{kj}(\mu)\right\} y_d^{ji}. \tag{20}$$

The rescaling of the field in Eq. (16) is absorbed into the Yukawa couplings. After the diagonalization of the mass matrices based on these couplings, it contributes to the CKM matrix as one-loop corrections. Since we only consider the charged current interaction in one-loop diagrams in the next section, these corrections lead to two-loop order effects and they are neglected.

The tree-level effective operator in Eq. (5) is also changed by the rescaling in Eq. (16):

$$\begin{aligned} i\frac{y_d^{j4}y_d^{i4*}}{M_4^2}\left(\overline{q_L^j}\phi\right)\not{D}_R^d\left(\phi^\dagger q_L^i\right) &= \left\{\delta^{kj} - \frac{1}{2}Z^{kj}(\mu)\right\} i\frac{y_d^{j4}y_d^{i4*}}{M_4^2}\left\{\delta^{il} - \frac{1}{2}Z^{il}(\mu)\right\}\left(\overline{q_L'^k}\phi\right)\not{D}_R^d\left(\phi^\dagger q_L'^l\right) \\ &\equiv i\frac{Y_d^{k4}Y_d^{l4*}}{M_4^2}\left(\overline{q_L'^k}\phi\right)\not{D}_R^d\left(\phi^\dagger q_L'^l\right), \end{aligned} \tag{21}$$

where we redefine the Yukawa coupling between the SM quarks and the VLQ as

$$Y_d^{k4} \equiv \left\{\delta^{kj} - \frac{1}{2}Z^{kj}(\mu)\right\} y_d^{j4}. \tag{22}$$

As we will see in the next subsection, this redefinition of the Yukawa coupling in Eq. (22) adds $\mathcal{O}(\frac{1}{16\pi^2 M_4^2})$ corrections to the CKM matrix and the FCNC coupling. In the next section we will take into account only leading-order contributions in $1/M_4^2$, and these corrections are neglected.

For the one-loop effective Lagrangian, the rescaling in Eq. (16) leads to two-loop order corrections and we can simply take $q_L' \simeq q_L$ in the one-loop effective Lagrangian.

2.2. *Electroweak symmetry breaking*

In this subsection, we derive the Lagrangian for the broken phase of the SM gauge symmetry. We substitute the following forms for the Higgs doublet in the Lagrangian Eqs. (6)–(11):

$$\phi = \begin{pmatrix} \chi^+ \\ (v + h + i\chi_0)/\sqrt{2} \end{pmatrix}, \tag{23}$$

$$\tilde{\phi} = \begin{pmatrix} (v + h - i\chi_0)/\sqrt{2} \\ -\chi^- \end{pmatrix}. \tag{24}$$

Here we do not take into account the running effect from the VLQ mass scale to the EW scale for the coefficients in the effective interactions in Eqs. (6)–(11). For the effective Lagrangian $\mathcal{L}_{\mathrm{Eff}}^{\mathrm{tree}}$ in Eq. (6), we obtain

$$\begin{aligned}\mathcal{L}_{\mathrm{Eff}}^{\mathrm{tree}} =& \frac{v^2}{4M_4^2}\left[h_d^{ji} m_d^{ik} \overline{d_L^j} d_R^k + \mathrm{h.c.}\right] + \frac{g}{2M_W}\cdot\frac{3v^2}{4M_4^2}\left[h_d^{ji} m_d^{ik} \overline{d_L^j} d_R^k (h + i\chi_0) + \mathrm{h.c.}\right] \\ & - \frac{g}{\sqrt{2}M_W}\cdot\frac{v^2}{4M_4^2}\left[h_d^{ji} m_u^{ii} \overline{d_L^j} u_R^i \chi^- + \mathrm{h.c.}\right] + \frac{g}{\sqrt{2}M_W}\cdot\frac{v^2}{2M_4^2}\left[h_d^{ji} m_d^{ik} \overline{u_L^j} d_R^k \chi^+ + \mathrm{h.c.}\right] \\ & + \frac{g}{\sqrt{2}}\cdot\frac{v^2}{4M_4^2}\left[h_d^{ji} \overline{u_L^j} \gamma^\mu d_L^i W_\mu^+ + \mathrm{h.c.}\right] - \frac{g}{2c_w}\cdot\frac{v^2}{2M_4^2} h_d^{ji} \overline{d_L^j} \gamma^\mu d_L^i Z_\mu + \cdots,\end{aligned} \tag{25}$$

where the ellipsis represents the terms including more than four fields, h_d^{ji} represents $y_d^{j4} y_d^{i4*}$, and c_w (s_w) denotes the cosine (sine) of the weak mixing angle θ_w. The mass matrices of the up-type and down-type quarks which correspond to $\mathcal{L}_{\mathrm{SM}}$ in Eq. (13) are denoted by $m_{u,d} \equiv v y_{u,d}/\sqrt{2}$. Adding the tree-level effective Lagrangian in Eq. (25) to the SM Lagrangian $\mathcal{L}_{\mathrm{SM}}$ in Eq. (13), the mass matrix of the down-type quarks changes into $\left(\delta^{ji} - \frac{v^2}{4M_4^2} h_d^{ji}\right) m_d^{ik}$. We diagonalize this mass matrix. At first, we introduce 3×3 unitary matrices K_L and K_R. These unitary matrices diagonalize the matrix m_d:

$$\begin{cases} d_L^i = K_L^{im} d_L^{\prime m} \\ d_R^i = K_R^{im} d_R^{\prime m} \end{cases} \quad \to \quad (K_L^\dagger m_d K_R)^{mn} \equiv m_d^{\prime m} \delta^{mn}, \tag{26}$$

where the prime indicates the mass basis of the SM. In this mass basis, the mass matrix of the down-type quarks changes into

$$K_L^{\dagger mj}\left(\delta^{ji} - \frac{v^2}{4M_4^2} h_d^{ji}\right) m_d^{ik} K_R^{kn} = \left(\delta^{mn} - \frac{v^2}{4M_4^2} h_d^{\prime mn}\right) m_d^{\prime n}, \tag{27}$$

where

$$(K_L^\dagger h_d K_L)^{mn} = K_L^{\dagger mj} y_d^{j4} y_d^{i4*} K_L^{in} \equiv y_d^{\prime m4} y_d^{\prime n4*} \equiv h_d^{\prime mn}. \tag{28}$$

The mass matrix in Eq. (27) is not diagonal. In order to diagonalize the mass matrix including the contributions of $\mathcal{O}(v^2/M_4^2)$, we introduce unitary matrices V_L and V_R,

$$\begin{cases} d_L^{\prime m} = V_L^{mp} d_L^{\prime\prime p} \\ d_R^{\prime m} = V_R^{mp} d_R^{\prime\prime p} \end{cases} \quad \to \quad V_L^{\dagger pm}\left(\delta^{mn} - \frac{v^2}{4M_4^2} h_d^{\prime mn}\right) m_d^{\prime n} V_R^{nq} \equiv m_d^{\prime\prime p} \delta^{pq}, \tag{29}$$

where the double prime denotes the mass basis of the model with VLQ. The physical masses of the down-type quarks are denoted by $m_d''^p = (m_d'', m_s'', m_b'')$. The mixing angles of these unitary matrices are of the order of $\mathcal{O}(v^2/M_4^2)$. Hereafter we omit the double prime on the quark fields of the mass basis and h_d denotes the h_d' in the right-hand side of Eq. (28). Finally, we obtain the following Lagrangian after the transformation in Eqs. (26) and (29):

$$\mathcal{L}_{\rm SM} + \mathcal{L}_{\rm Eff}^{\rm tree} = \mathcal{L}_0 + \mathcal{L}_A + \mathcal{L}_W + \mathcal{L}_Z + \mathcal{L}_{\chi^\pm} + \mathcal{L}_h + \mathcal{L}_{\chi_0} + \cdots, \tag{30}$$

where the ellipsis represents the terms that contain more than four fields. Each part of the Lagrangians is given below:

$$\mathcal{L}_0 = \overline{u^i} i\partial\!\!\!/ u^i + \overline{d^p} i\partial\!\!\!/ d^p - \left[m_u^i \overline{u^i} u^i + m_d^p \overline{d^p} d^p\right], \tag{31}$$

$$\mathcal{L}_A = -e\left[Q_u \overline{u^i}\gamma^\mu u^i + Q_d \overline{d^p}\gamma^\mu d^p\right] A_\mu, \tag{32}$$

$$\mathcal{L}_W = -\frac{g}{\sqrt{2}} \overline{u^i}\gamma^\mu V_{\rm CKM}^{iq} L d^q W_\mu^+ + \text{h.c.}, \tag{33}$$

$$\mathcal{L}_Z = -\frac{g}{c_w}\left[\overline{u^i}\gamma^\mu\left(\frac{1}{2}L - Q_u s_w^2\right)u^i - \overline{d^p}\gamma^\mu\left(\frac{1}{2}Z_{\rm NC}^{pq} L + Q_d s_w^2 \delta^{pq}\right)d^q\right] Z_\mu, \tag{34}$$

$$\mathcal{L}_{\chi^\pm} = \frac{g}{\sqrt{2}M_W}\overline{u^i} V_{\rm CKM}^{ip}\left(m_u^i L - m_d^p R\right) d^p \chi^+ + \text{h.c.}, \tag{35}$$

$$\mathcal{L}_h = -\frac{g}{2M_W}\overline{d^p} Z_{\rm NC}^{pq}\left(m_d^q R + m_d^p L\right) d^q h, \tag{36}$$

$$\mathcal{L}_{\chi_0} = -\frac{ig}{2M_W}\overline{d^p} Z_{\rm NC}^{pq}\left(m_d^q R - m_d^p L\right) d^q \chi_0. \tag{37}$$

In Eqs. (31)–(37), L and R denote the chiral projection operators, $L \equiv \frac{1-\gamma_5}{2}, R \equiv \frac{1+\gamma_5}{2}$. The electromagnetic charges of up-type and down-type quarks are denoted by Q_u and Q_d, respectively. The 3×3 CKM matrix $V_{\rm CKM}$ is defined as

$$V_{\rm CKM} \equiv K_L\left(1 - \frac{v^2}{4M_4^2} h_d\right) V_L. \tag{38}$$

The FCNCs arise from the 3×3 non-diagonal matrix $Z_{\rm NC}$ in the Z, h, and χ_0 interactions in Eqs. (34), (36), and (37). The matrix Z_{NC} in the neutral currents is defined as follows:

$$Z_{\rm NC} \equiv V_L^\dagger\left(1 - \frac{v^2}{2M_4^2} h_d\right) V_L \simeq 1 - \frac{v^2}{2M_4^2} h_d + \mathcal{O}(v^4/M_4^4). \tag{39}$$

Using Eqs. (38) and (39), we obtain the relation between the CKM matrix $V_{\rm CKM}$ and the matrix $Z_{\rm NC}$ up to $\mathcal{O}(v^2/M_4^2)$:

$$\sum_{i=u,c,t} V_{\rm CKM}^{ip*} V_{\rm CKM}^{iq} = Z_{\rm NC}^{pq}. \tag{40}$$

Equation (40) shows that the unitarity of the CKM matrix for the three generations does not hold due to the deviation from the unit matrix of the matrix $Z_{\rm NC}$ in Eq. (39). Taking the limit of $M_4 \to \infty$, the unitarity relation is restored.

Next we rewrite the one-loop level effective Lagrangian Eqs. (8)–(11) in terms of the mass basis defined in Eq. (29). Below we write the part of the dipole operators and omit the other parts of the effective Lagrangian:

$$\begin{aligned}
\mathcal{L}^B_{\text{Eff}} + \mathcal{L}^W_{\text{Eff}} = &\frac{g}{16\pi^2 c_w}\cdot\frac{G_F}{6\sqrt{2}}\left(1-\frac{7}{2}Q_u s_w^2\right)\overline{u^j_L}V^{jp}_{\text{CKM}}\left(\delta^{pq}-Z^{pq}_{\text{NC}}\right)V^{iq*}_{\text{CKM}}m^i_u\sigma_{\mu\nu}u^i_R Z^{\mu\nu}\\
&+\frac{g}{16\pi^2 c_w}\cdot\frac{G_F}{6\sqrt{2}}\left(-1+Q_d s_w^2\right)\overline{d^p_L}\left(\delta^{pq}-Z^{pq}_{\text{NC}}\right)m^q_d\sigma_{\mu\nu}d^q_R Z^{\mu\nu}\\
&+\frac{e}{16\pi^2}\cdot\frac{7G_F}{12\sqrt{2}}Q_u\overline{u^j_L}V^{jp}_{\text{CKM}}\left(\delta^{pq}-Z^{pq}_{\text{NC}}\right)V^{iq*}_{\text{CKM}}m^i_u\sigma_{\mu\nu}u^i_R F^{\mu\nu}_A\\
&-\frac{e}{16\pi^2}\cdot\frac{G_F}{6\sqrt{2}}Q_d\overline{d^p_L}\left(\delta^{pq}-Z^{pq}_{\text{NC}}\right)m^q_d\sigma_{\mu\nu}d^q_R F^{\mu\nu}_A\\
&+\frac{g}{16\sqrt{2}\pi^2}\cdot\frac{G_F}{3\sqrt{2}}\overline{d^p_L}\left(\delta^{pq}-Z^{pq}_{\text{NC}}\right)V^{iq*}_{\text{CKM}}m^i_u\sigma_{\mu\nu}u^i_R W^{-\mu\nu}\\
&+\frac{g}{16\sqrt{2}\pi^2}\cdot\frac{G_F}{3\sqrt{2}}\overline{u^j_L}V^{jp}_{\text{CKM}}\left(\delta^{pq}-Z^{pq}_{\text{NC}}\right)m^q_d\sigma_{\mu\nu}d^q_R W^{+\mu\nu}+\text{h.c.},
\end{aligned}\tag{41}$$

$$\begin{aligned}
\mathcal{L}^G_{\text{Eff}} = &-\frac{g_s}{16\pi^2}\cdot\frac{G_F}{6\sqrt{2}}\overline{u^j_L}V^{jp}_{\text{CKM}}\left(\delta^{pq}-Z^{pq}_{\text{NC}}\right)V^{iq*}_{\text{CKM}}m^i_u\frac{\lambda^a}{2}\sigma_{\mu\nu}u^i_R G^{a\mu\nu}\\
&-\frac{g_s}{16\pi^2}\cdot\frac{G_F}{6\sqrt{2}}\overline{d^p_L}\left(\delta^{pq}-Z^{pq}_{\text{NC}}\right)m^q_d\frac{\lambda^a}{2}\sigma_{\mu\nu}d^q_R G^{a\mu\nu}+\text{h.c.},
\end{aligned}\tag{42}$$

where the field strengths $Z^{\mu\nu}$, $F^{\mu\nu}_A$, and $W^{\pm\mu\nu}$ are defined as

$$Z^{\mu\nu}=\partial^\mu Z^\nu-\partial^\nu Z^\mu,\quad F^{\mu\nu}_A=\partial^\mu A^\nu-\partial^\nu A^\mu,\quad W^{\pm\mu\nu}=\partial^\mu W^{\pm\nu}-\partial^\nu W^{\pm\mu},\tag{43}$$

respectively. Note that the coefficient of the photon dipole operator with the down-type quarks is consistent with the case of the full theory calculation up to $\mathcal{O}(M_4^{-2})$ [25].

3. Effective Lagrangian for $\Delta B = 1, 2$ and $b \to s\gamma^{(*)}$ processes

In order to analyze the B meson system, we derive the effective Lagrangian for the $\Delta B = 1, 2$ and $b \to s\gamma^{(*)}$ processes in the model with VLQ. Here we focus on contributions derived from the effective Lagrangian in Eq. (30). There are three sources for the effective Lagrangian. The first contribution is the same as the case of the SM. The second contribution corresponds to the diagrams that include the FCNC couplings. The third contribution comes from the violation of CKM unitarity. In the following computations, we use the 't Hooft–Feynman gauge.

3.1. $\Delta B = 1$ *process*

First we consider the $\Delta B = 1$ process to calculate the branching ratio of the $B_s \to \mu^+\mu^-$ process in the next section. The diagrams that contribute to the effective Lagrangian up to $\mathcal{O}(Z_{\text{NC}})$ are shown in Fig. 3.

The $\bar{b}s \to \mu^+\mu^-$ process occurs at tree level in the model with VLQ since there is the tree-level Z FCNC among the down-type quarks. In one-loop level, the contribution comes from the Feynman diagrams in Figs. 3(*a*) and (*b*) that are also present in the SM. However, these amplitudes include

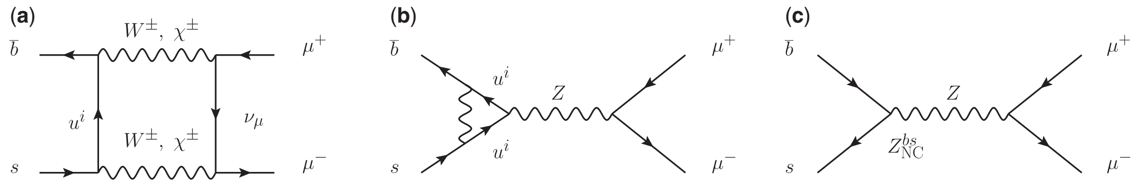

Fig. 3. The Feynman diagrams that contribute to the $\bar{b}s \to \mu^+\mu^-$ process. Diagrams (*a*) and (*b*) are the same contributions as the SM. Diagram (*c*) is the new contribution in the model with VLQ.

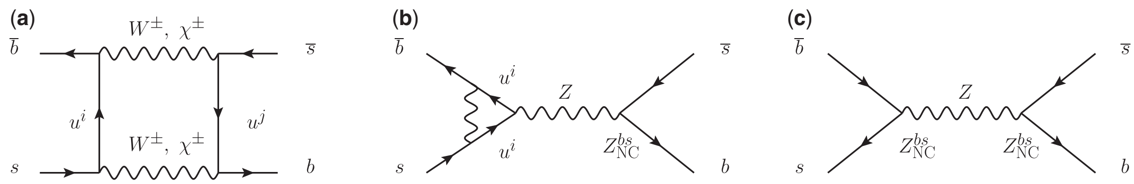

Fig. 4. The Feynman diagrams that contribute to the $\Delta B = 2$ process in the model with VLQ. Diagram (*a*) is same as in the case of the SM, but the additional contribution arises from Diagram (*a*) by the violation of CKM unitarity.

the additional contributions due to the violation of CKM unitarity. Since these contributions are suppressed by the loop factor $e^2/(16\pi^2)$ compared with the contribution of the tree diagram in Fig. 3(*c*), we neglect the contribution from the violation of CKM unitarity in the computation of the $\bar{b}s \to \mu^+\mu^-$ process. Then the effective Lagrangian for $\bar{b}s \to \mu^+\mu^-$ is given as follows:

$$\mathcal{L}_{\rm Eff}(\bar{b}s \to \mu^+\mu^-) = \frac{\sqrt{2}G_F\alpha_{em}}{\pi s_w^2}\lambda_{bs}^t Y_0(x_t)\left\{1 - \frac{\pi s_w^2}{\alpha_{em}Y_0(x_t)} \cdot \frac{Z_{\rm NC}^{bs}}{\lambda_{bs}^t}\right\}\left[\overline{b_L}\gamma^\mu s_L\right]\left[\overline{\mu_L}\gamma_\mu\mu_L\right], \quad (44)$$

where $\lambda_{bs}^t \equiv V_{\rm CKM}^{tb*}V_{\rm CKM}^{ts}$, and $\alpha_{em} = e^2/(4\pi)$ denotes the fine structure constant of the electromagnetic interaction. The Inami–Lim function $Y_0(x_t)$ is [26,27]

$$Y_0(x_i) = \frac{1}{8}x_i - \frac{3}{8}\frac{x_i}{x_i - 1} + \frac{3}{8}\frac{x_i^2}{(x_i - 1)^2}\ln x_i, \quad (45)$$

where $x_i \equiv (m_u^i/M_W)^2$. The first term in Eq. (44) comes from the diagrams in Figs. 3(*a*) and (*b*) with the CKM unitarity relation for the SM ($\sum_{i=u,c,t}\lambda_{bs}^i = 0$), that is, the SM contribution. The second term of Eq. (44) comes from the diagram in Fig. 3(*c*), so this term is the new contribution in the model with VLQ.

3.2. $\Delta B = 2$ process

Next we show the effective Lagrangian for the $\Delta B = 2$ process in order to compute the mass difference of the B_s meson in a later section. In Refs. [28–31], the $\Delta B = 2$ process was computed up to $\mathcal{O}(Z_{\rm NC}^2)$ and $\mathcal{O}(Z_{\rm NC} \cdot \alpha_{em}/(4\pi))$. The diagrams that contribute to the $\Delta B = 2$ process are given in Fig. 4.

From the diagrams in Fig. 4, we obtain the effective Lagrangian for the $\bar{b}s \leftrightarrow \bar{s}b$ process as [28–31]:

$$\mathcal{L}_{\rm Eff}(\bar{b}s \leftrightarrow \bar{s}b) = \frac{G_F}{\sqrt{2}}\frac{\alpha_{em}}{4\pi s_w^2}\left(\lambda_{bs}^t\right)^2 S_0(x_t)$$
$$\times\left\{1 + \frac{8Y_0(x_t)}{S_0(x_t)} \cdot \frac{Z_{\rm NC}^{bs}}{\lambda_{bs}^t} - \frac{4\pi s_w^2}{\alpha_{em}S_0(x_t)}\left(\frac{Z_{\rm NC}^{bs}}{\lambda_{bs}^t}\right)^2\right\}\left[\overline{b_L}\gamma^\mu s_L\right]\left[\overline{b_L}\gamma_\mu s_L\right], \quad (46)$$

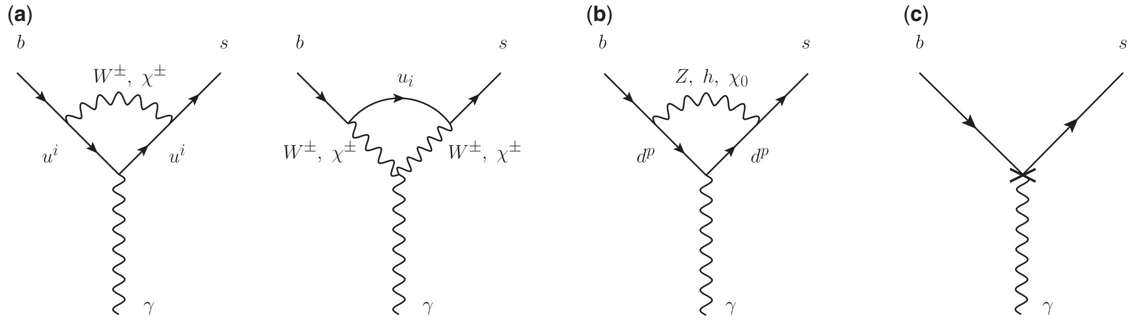

Fig. 5. The Feynman diagrams that contribute to the $b \to s\gamma^{(*)}$ process. The diagrams in (a) are the same contributions as the SM. The additional contribution arises from the diagrams in (a) by the violation of CKM unitarity. Diagram (b) is the new contribution in the model with VLQ. Diagram (c) is the counterterm determined by the quark self-energy and Z–photon, χ_0–photon mixing diagrams in Fig. 6.

where

$$S_0(x_i) = -\frac{3}{2}\left(\frac{x_i}{x_i - 1}\right)^3 \ln x_i - x_i \left\{\frac{1}{4} - \frac{9}{4}\frac{1}{x_i - 1} - \frac{3}{2}\frac{1}{(x_i - 1)^2}\right\} \tag{47}$$

is the Inami–Lim function [26]. Also, $Y_0(x_t)$ is given in Eq. (45). The first term in Eq. (46) comes from the diagram in Fig. 4(a) with the CKM unitarity relation. The second term in Eq. (46) is obtained from the violation of CKM unitarity in the diagram in Fig. 4(a) in addition to the contribution from the diagram in Fig. 4(b). The CKM unitarity relation is used for the one-loop Z FCNC vertex in Fig. 4(b) since the $\mathcal{O}(Z_{\rm NC}^2 \cdot \alpha_{em}/(4\pi))$ contribution is neglected. The third term comes from the diagram in Fig. 4(c). Note that the effective Lagrangian in Eq. (46) contains only the Inami–Lim functions which are gauge-parameter independent [31].

3.3. $b \to s\gamma^{(*)}$ process

Finally we derive the effective Lagrangian for the $b \to s\gamma^{(*)}$ process to evaluate the $\bar{B}$ meson radiative decay $\bar{B} \to X_s\gamma$. In addition to the contribution from the effective Lagrangian in Eq. (41), the diagrams in Fig. 5 also contribute to the $b \to s\gamma^{(*)}$ process. The effective Lagrangian for the $b \to s\gamma$ process has been calculated in terms of the full theory [25,32], while the effective Lagrangian for the $b \to s\gamma^*$ process has not been calculated. Here we will give the effective Lagrangian for both $b \to s\gamma$ and $b \to s\gamma^*$ in terms of the effective theory.

In the model with VLQ, there are no FCNCs by the quark–quark–photon interaction at tree level. Therefore the leading-order contributions that contain the FCNC couplings come from the violation of CKM unitarity in the diagrams in Fig. 5(a) and the one-loop diagram in Fig. 5(b) [25,32]. In order to obtain the effective Lagrangian for the $b \to s\gamma^{(*)}$ process, we compute the amplitudes of the diagrams in Fig. 5. We introduce several counterterms when we renormalize amplitudes for Figs. 5(a) and (b). As mentioned in Ref. [25], the counterterms of the renormalization for the quark fields remove the divergence of the diagrams in Fig. 5(a) with the CKM unitarity and that of the diagram in Fig. 5(b). However, these counterterms cannot remove all the divergence arising from these diagrams. There still remains the divergence that comes from the violation of CKM unitarity in Fig. 5(a). Therefore we have to introduce another counterterm. We consider the renormalization for the neutral gauge bosons Z and A [33]. The bare fields Z_0^μ and A_0^μ are related to the renormalized fields as follows:

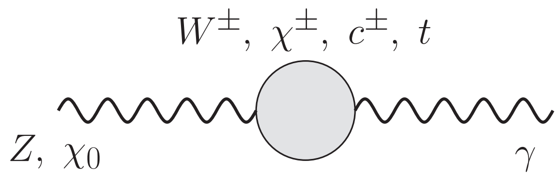

Fig. 6. The diagram where a photon mixes with a Z or χ_0 at one-loop level. $c^{\pm}$ denotes the Faddeev–Popov ghost.

$$\begin{pmatrix} Z_0^{\mu} \\ A_0^{\mu} \end{pmatrix} = \begin{pmatrix} \sqrt{Z_{\rm ZZ}} & \sqrt{Z_{\rm ZA}} \\ \sqrt{Z_{\rm AZ}} & \sqrt{Z_{\rm AA}} \end{pmatrix} \begin{pmatrix} Z^{\mu} \\ A^{\mu} \end{pmatrix}, \tag{48}$$

where $\sqrt{Z_{ij}}$ $(i,j = Z, A)$ are the renormalization constants. The divergence coming from the violation of CKM unitarity in the diagrams in Fig. 5(a) is exactly cancelled by the counterterm given as

$$Z_{\rm NC}^{sb}\bar{s}\gamma_{\mu}LbZ_0^{\mu} \quad \rightarrow \quad \sqrt{Z_{\rm ZA}} \cdot Z_{\rm NC}^{sb}\bar{s}\gamma_{\mu}LbA^{\mu}. \tag{49}$$

The renormalization constants $\sqrt{Z_{\rm ZA}}$ and $\sqrt{Z_{\rm AZ}}$ are determined by the diagrams in Fig. 6, where the Z (or χ_0) and photon mix at one-loop level.

The finite part of the transition amplitude of the diagram in Fig. 6 contributes to the effective Lagrangian for the $b \rightarrow s\gamma^*$ process. Finally, we can obtain the effective Lagrangian $\mathcal{L}_{\rm Eff}(b \rightarrow s\gamma)$ for the on-shell photon and the effective Lagrangian $\mathcal{L}_{\rm Eff}(b \rightarrow s\gamma^*)$ that vanishes for the on-shell photon as follows:

$$\mathcal{L}_{\rm Eff}(b \rightarrow s\gamma) = \mathcal{L}_{\rm Eff}^{\rm CC}(b \rightarrow s\gamma) + \mathcal{L}_{\rm Eff}^{\rm uv}(b \rightarrow s\gamma) + \mathcal{L}_{\rm Eff}^{\rm NC}(b \rightarrow s\gamma), \tag{50}$$

$$\mathcal{L}_{\rm Eff}(b \rightarrow s\gamma^*) = \mathcal{L}_{\rm Eff}^{\rm CC}(b \rightarrow s\gamma^*) + \mathcal{L}_{\rm Eff}^{\rm uv}(b \rightarrow s\gamma^*) + \mathcal{L}_{\rm Eff}^{\rm NC}(b \rightarrow s\gamma^*) + \mathcal{L}_{\rm Eff}^{\rm Mix}(b \rightarrow s\gamma^*), \tag{51}$$

where the indices "CC" denote the contributions from the diagrams in Fig. 5(a) with the CKM unitarity relation, namely the SM contributions. Also, the indices "uv" and "NC" imply the contributions from the violation of CKM unitarity and the diagram in Fig. 5(b), which include the neutral current respectively. The index "Mix" indicates the contributions from the Z–photon and χ_0–photon mixing diagrams. Concretely, these effective Lagrangian are obtained as:

$$\mathcal{L}_{\rm Eff}^{\rm CC}(b \rightarrow s\gamma) = -\frac{G_F e}{8\sqrt{2}\pi^2}\sum_{i=c,t}\lambda_{sb}^{i}\left\{Q_u F_u(x_i) + F_W(x_i)\right\}\bar{s}\sigma_{\mu\nu}\left(m_b R + m_s L\right) bF_A^{\mu\nu}, \tag{52}$$

$$\mathcal{L}_{\rm Eff}^{\rm uv}(b \rightarrow s\gamma) = \frac{G_F e}{8\sqrt{2}\pi^2}Z_{\rm NC}^{sb}\left(\frac{2}{3}Q_u + \frac{5}{6}\right)\bar{s}\sigma_{\mu\nu}\left(m_b R + m_s L\right) bF_A^{\mu\nu}, \tag{53}$$

$$\begin{aligned}\mathcal{L}_{\rm Eff}^{\rm NC}(b \rightarrow s\gamma) = \frac{G_F e}{8\sqrt{2}\pi^2}Q_d &\sum_{p=d,s,b}\Big\{Z_{\rm NC}^{sp}Z_{\rm NC}^{pb}F_{\rm ZZ}(r_p, w_p) \\ &+Z_{\rm NC}^{sb}Q_d s_w^2(\delta^{sp} + \delta^{pb})F_{\rm Z}(r_p)\Big\}\bar{s}\sigma_{\mu\nu}\left(m_b R + m_s L\right) bF_A^{\mu\nu} \\ &- \frac{G_F e}{4\sqrt{2}\pi^2}Q_d\sum_{p=s,b}Z_{\rm NC}^{sb}Q_d s_w^2 F'_{\rm Z}(r_p)\bar{s}\sigma_{\mu\nu}\left(\delta^{pb}m_b R + \delta^{sp}m_s L\right) bF_A^{\mu\nu},\end{aligned} \tag{54}$$

and

$$\mathcal{L}^{\rm CC}_{\rm Eff}(b\to s\gamma^*) = -\frac{G_F e}{8\sqrt{2}\pi^2}\sum_{i=c,t}\lambda^i_{sb}\left\{Q_u f_u(x_i) + f_W(x_i)\right\}\bar{s}\gamma_\nu L b\partial_\mu F^{\mu\nu}_A, \tag{55}$$

$$\mathcal{L}^{\rm uv}_{\rm Eff}(b\to s\gamma^*) = -\frac{G_F e}{8\sqrt{2}\pi^2}Z^{sb}_{\rm NC}\left\{Q_u\left(-\frac{2}{9}+\frac{4}{3}\ln x_u\right)-\frac{16}{9}\right\}\bar{s}\gamma_\nu L b\partial_\mu F^{\mu\nu}_A, \tag{56}$$

$$\begin{aligned}\mathcal{L}^{\rm NC}_{\rm Eff}(b\to s\gamma^*) = \frac{G_F e}{8\sqrt{2}\pi^2}Q_d\sum_{p=d,s,b}&\Big\{Z^{sp}_{\rm NC}Z^{pb}_{\rm NC}f_{\rm ZZ}(r_p,w_p)\\ &+Z^{sb}_{\rm NC}Q_d s^2_w\left(\delta^{sp}+\delta^{pb}\right)f_{\rm Z}(r_p)\Big\}\bar{s}\gamma_\nu L b\partial_\mu F^{\mu\nu}_A,\end{aligned} \tag{57}$$

$$\begin{aligned}\mathcal{L}^{\rm Mix}_{\rm Eff}(b\to s\gamma^*) = \frac{G_F e}{8\sqrt{2}\pi^2}Z^{sb}_{\rm NC}&\left\{\left(10c^2_w+\frac{1}{3}\right)\ln\frac{\mu^2}{M^2_W}+\frac{4}{3}c^2_w\right.\\ &\left.-2Q_u\left(1-4Q_u s^2_w\right)\ln\frac{\mu^2}{m^2_t}\right\}\bar{s}\gamma_\nu L b\partial_\mu F^{\mu\nu}_A.\end{aligned} \tag{58}$$

The Inami–Lim functions in Eqs. (52) and (55) are given as follows [26]:

$$F_u(x_i) \equiv \frac{x_i(2+3x_i-6x_i^2+x_i^3+6x_i\ln x_i)}{4(x_i-1)^4}, \tag{59}$$

$$F_W(x_i) \equiv \frac{x_i(1-6x_i+3x_i^2+2x_i^3-6x_i^2\ln x_i)}{4(x_i-1)^4}, \tag{60}$$

$$f_u(x_i) \equiv -\frac{x_i\{18-29x_i+10x_i^2+x_i^3+(32-18x_i)\ln x_i\}}{6(x_i-1)^4}+\frac{4}{3(x_i-1)^4}\ln x_i-\frac{4}{3}\ln x_u, \tag{61}$$

$$f_W(x_i) \equiv \frac{x_i\{12-11x_i-8x_i^2+7x_i^3+2x_i(12-10x_i+x_i^2)\ln x_i\}}{6(x_i-1)^4}, \tag{62}$$

where the subscripts "u" and "W" indicate the contributions that are proportional to the electromagnetic charge of the up-type quarks and the W boson respectively. The functions $F_{\rm ZZ}$, $F_{\rm Z}$, and $F'_{\rm Z}$ in Eq. (54) are given as[1]

$$F_{\rm ZZ}(r_p,w_p) \equiv F_1(r_p)+F_2(r_p)+F_3(w_p), \tag{63}$$

$$F_{\rm Z}(r_p) \equiv 2F_1(r_p), \tag{64}$$

$$F'_{\rm Z}(r_p) \equiv \frac{1-r_p^2+2r_p\ln r_p}{(1-r_p)^3}, \tag{65}$$

[1] The terms linear to $Z^{sb}_{\rm NC}$ in Eq. (54) and the loop functions $F_Z(r_p)$ and $F'_Z(r_p)$ in Eqs. (64) and (65) do not agree with the corresponding terms of Eqs. (23) and (24) and the loop function $F^{\rm NC}_1(r_\alpha)$ of Ref. [25].

where $r_p \equiv (m_d^p/M_Z)^2$ and $w_p \equiv (m_d^p/M_h)^2$. The functions F_1, F_2, and F_3,

$$F_1(r_p) \equiv \frac{4 - 9r_p + 5r_p^3 + 6r_p(1-2r_p)\ln r_p}{12(1-r_p)^4}, \tag{66}$$

$$F_2(r_p) \equiv r_p \frac{-20 + 39r_p - 24r_p^2 + 5r_p^3 + 6(-2+r_p)\ln r_p}{24(1-r_p)^4}, \tag{67}$$

$$F_3(w_p) \equiv -w_p \frac{-16 + 45w_p - 36w_p^2 + 7w_p^3 + 6(-2+3w_p)\ln w_p}{24(1-w_p)^4}, \tag{68}$$

come from the diagram Fig. 5(b) where the exchanged particles are Z, χ_0, and h, respectively. The functions f_{ZZ} and f_{Z} in Eq. (57) are obtained as follows:

$$f_{\mathrm{ZZ}}(r_p, w_p) \equiv f_1(r_p) + f_2(r_p) + f_3(w_p), \tag{69}$$

$$f_{\mathrm{Z}}(r_p) \equiv 2f_1(r_p), \tag{70}$$

where

$$f_1(r_p) \equiv \frac{2 + 27r_p - 54r_p^2 + 25r_p^3 - 6(2 - 9r_p + 6r_p^2)\ln r_p}{18(1-r_p)^4}, \tag{71}$$

$$f_2(r_p) \equiv r_p \frac{-16 + 45r_p - 36r_p^2 + 7r_p^3 + 6(-2+3r_p)\ln r_p}{36(1-r_p)^4}, \tag{72}$$

$$f_3(w_p) \equiv f_2(w_p). \tag{73}$$

The effective Lagrangians for the $b \to sg^{(*)}$ process can be obtained by replacing the external photon line which attached to quarks with the gluon line in Fig. 5. They are obtained as follows:

$$\mathcal{L}_{\mathrm{Eff}}^{\mathrm{CC}}(b \to sg) = -\frac{G_F g_s}{8\sqrt{2}\pi^2} \sum_{i=c,t} \lambda_{sb}^i F_u(x_i) \bar{s}\sigma_{\mu\nu}(m_b R + m_s L)\frac{\lambda^a}{2} b G^{a\mu\nu}, \tag{74}$$

$$\mathcal{L}_{\mathrm{Eff}}^{\mathrm{uv}}(b \to sg) = \frac{G_F g_s}{8\sqrt{2}\pi^2} \cdot \frac{2}{3} Z_{\mathrm{NC}}^{sb} \bar{s}\sigma_{\mu\nu}(m_b R + m_s L)\frac{\lambda^a}{2} b G^{a\mu\nu}, \tag{75}$$

$$\begin{aligned}\mathcal{L}_{\mathrm{Eff}}^{\mathrm{NC}}(b \to sg) = {} & \frac{G_F g_s}{8\sqrt{2}\pi^2} \sum_{p=d,s,b} \Big\{ Z_{\mathrm{NC}}^{sp} Z_{\mathrm{NC}}^{pb} F_{\mathrm{ZZ}}(r_p, w_p) \\ & + Z_{\mathrm{NC}}^{sb} Q_d s_w^2 (\delta^{sp} + \delta^{pb}) F_{\mathrm{Z}}(r_p) \Big\} \bar{s}\sigma_{\mu\nu}(m_b R + m_s L)\frac{\lambda^a}{2} b G^{a\mu\nu} \\ & - \frac{G_F g_s}{4\sqrt{2}\pi^2} \sum_{p=s,b} Z_{\mathrm{NC}}^{sb} Q_d s_w^2 F'_{\mathrm{Z}}(r_p) \bar{s}\sigma_{\mu\nu}\left(\delta^{pb} m_b R + \delta^{sp} m_s L\right)\frac{\lambda^a}{2} b G^{a\mu\nu},\end{aligned} \tag{76}$$

and

$$\mathcal{L}^{\mathrm{CC}}_{\mathrm{Eff}}(b \to sg^*) = -\frac{G_F g_s}{8\sqrt{2}\pi^2} \sum_{i=c,t} \lambda^i_{sb} f_u(x_i) \bar{s}\gamma_\nu L \frac{\lambda^a}{2} b \partial_\mu G^{a\mu\nu}, \tag{77}$$

$$\mathcal{L}^{\mathrm{uv}}_{\mathrm{Eff}}(b \to sg^*) = -\frac{G_F g_s}{8\sqrt{2}\pi^2} Z^{sb}_{\mathrm{NC}} \left(-\frac{2}{9} + \frac{4}{3}\ln x_u\right) \bar{s}\gamma_\nu L \frac{\lambda^a}{2} b \partial_\mu G^{a\mu\nu}, \tag{78}$$

$$\mathcal{L}^{\mathrm{NC}}_{\mathrm{Eff}}(b \to sg^*) = \frac{G_F g_s}{8\sqrt{2}\pi^2} \sum_{p=d,s,b} \Big\{ Z^{sp}_{\mathrm{NC}} Z^{pb}_{\mathrm{NC}} f_{ZZ}(r_p, w_p) + Z^{sb}_{\mathrm{NC}} Q_d s^2_w \left(\delta^{sp} + \delta^{pb}\right) f_Z(r_p) \Big\} \bar{s}\gamma_\nu L \frac{\lambda^a}{2} b \partial_\mu G^{a\mu\nu}. \tag{79}$$

4. Analysis of B_s–$\overline{B_s}$ mass difference, $B_s \to \mu^+\mu^-$ and $\bar{B} \to X_s\gamma$ processes, and violation of CKM unitarity

In this section, we will make numerical calculations for the mass difference of the B_s meson ΔM_{B_s}, the branching ratio of $B_s \to \mu^+\mu^-$ and the branching ratio of the inclusive radiative decay of the $\bar{B}$ meson $\bar{B} \to X_s\gamma$ in the model with VLQ. In addition to these processes, we consider the constraint from Eq. (40). We will use the new physics parameters defined as

$$r_{sb} \equiv \left|\frac{Z^{sb}_{\mathrm{NC}}}{\lambda^t_{sb}}\right|, \quad \theta_{sb} \equiv \arg\left[\frac{Z^{sb}_{\mathrm{NC}}}{\lambda^t_{sb}}\right] \tag{80}$$

in the following computations.

4.1. B_s–$\overline{B_s}$ mass difference

We can obtain the mass difference of the B_s meson in the model with VLQ as [28–31]:

$$\Delta M_{B_s} = \frac{G_F}{\sqrt{2}} \frac{\alpha_{em}}{6\pi s^2_w} \eta_B B_s f^2_{B_s} m_{B_s} |S_0(x_t)| \left|\lambda^t_{sb}\right|^2 |\Delta_1(r_{sb}, \theta_{sb})|, \tag{81}$$

where η_B, B_s, and f_{B_s} represent the QCD factor, the bag parameter of the B_s meson, and the B_s meson decay constant, respectively. Here we use the QCD correction of the SM. The numerical values for the parameters in Eq. (81) are shown in Table 1.

Table 1. The input parameter values.

$\alpha^{-1}_{em}(m_b \sim M_W)$	130.3 ± 2.3	[40]	$\alpha_s(M_Z)$	0.1181 ± 0.0011	[44]
M_W	80.385 ± 0.015 GeV	[44]	M_Z	91.1876 ± 0.0021 GeV	[44]
G_F	1.16638×10^{-5} GeV^{-2}	[44]	$\sin\theta_w$	0.23129	[44]
$m_{c,\overline{\mathrm{MS}}}$	1.28 ± 0.03 GeV	[44]	$m_{b,\overline{\mathrm{MS}}}$	$4.18^{+0.04}_{-0.03}$ GeV	[44]
$m_{t,\mathrm{pole}}$	173.5 ± 1.1 GeV	[44]	m_μ	105.6584 MeV	[44]
m_B	5.27963 ± 0.00015 GeV	[44]	m_{B_s}	5.36689 ± 0.00019 GeV	[44]
τ_{B_s}	$(1.505 \pm 0.005) \times 10^{-12}$ s	[44]	ΔM_{B_s}	$(1.1688 \pm 0.0014) \times 10^{-8}$ MeV	[44]
$\mathrm{Br}[\bar{B} \to X_c e\overline{\nu_e}]_{\mathrm{Exp}}$	$(10.1 \pm 0.4) \times 10^{-2}$	[44]	η_Y	1.0113	[35]
η_B	0.5510 ± 0.0022	[34]	f_{B_s}	$225.1 \pm 1.5 \pm 2.0$ MeV	[5]
B_s	$1.320 \pm 0.016 \pm 0.030$	[5]	V_{us}	$0.22508^{+0.00030}_{-0.00028}$	[5]
V_{ub}	$0.003715^{+0.000060}_{-0.000060}$	[5]	V_{cs}	$0.973471^{+0.000067}_{-0.000067}$	[5]
V_{cb}	$0.04181^{+0.00028}_{-0.00060}$	[5]			

The function $\Delta_1(r_{sb},\theta_{sb})$ is given as

$$|\Delta_1(r_{sb},\theta_{sb})| = \left[1+\frac{16Y_0(x_t)}{S_0(x_t)}r_{sb}\cos\theta_{sb}+\left\{\left|\frac{8Y_0(x_t)}{S_0(x_t)}\right|^2-\frac{8\pi s_w^2}{\alpha_{em}S_0(x_t)}\cos 2\theta_{sb}\right\}r_{sb}^2\right.$$
$$\left.-\frac{64\pi s_w^2}{\alpha_{em}S_0(x_t)}\frac{Y_0(x_t)}{S_0(x_t)}r_{sb}^3\cos\theta_{sb}+\left|\frac{4\pi s_w^2}{\alpha_{em}S_0(x_t)}\right|^2 r_{sb}^4\right]^{\frac{1}{2}}. \tag{82}$$

We cannot use the SM value for the product of the CKM matrix elements $|\lambda_{sb}^t|$ in the model with VLQ since the new physics parameters r_{sb} and θ_{sb} affect the determination of the CKM matrix elements. Instead, we determine $|\lambda_{sb}^t|$ by using Eq. (81) in the following computations. Therefore, $|\lambda_{sb}^t|$ is obtained as a function with respect to the new physics parameters r_{sb} and θ_{sb}.

4.2. *Branching ratio of $B_s \to \mu^+\mu^-$*

The branching ratio of the $B_s \to \mu^+\mu^-$ process in the model with VLQ is given as follows:

$$\mathrm{Br}\left[B_s\to\mu^+\mu^-\right]_{\mathrm{VLQ}}$$
$$=\tau_{B_s}\frac{G_F^2}{16\pi}\left(\frac{\alpha_{em}}{\pi s_w^2}\right)^2|\eta_Y Y_0(x_t)|^2\left|f_{B_s}\right|^2 m_{B_s}m_\mu^2\sqrt{1-\frac{4m_\mu^2}{m_{B_s}^2}}\left|\lambda_{sb}^t\right|^2|\Delta_2(r_{sb},\theta_{sb})|^2, \tag{83}$$

where η_Y is the next-to-leading-order (NLO) QCD correction [34,35]. The lifetime of the B_s meson is denoted by τ_{B_s}. These values are shown in Table 1. The function $\Delta_2(r_{sb},\theta_{sb})$ is

$$|\Delta_2(r_{sb},\theta_{sb})| = \left[1-\frac{2\pi s_w^2}{\alpha_{em}Y_0(x_t)}r_{sb}\cos\theta_{sb}+\left\{\frac{\pi s_w^2}{\alpha_{em}Y_0(x_t)}\right\}^2 r_{sb}^2\right]^{\frac{1}{2}}. \tag{84}$$

4.3. *Branching ratio of $\bar{B}\to X_s\gamma$*

The $\bar{B}$ meson inclusive radiative decay $\bar{B}\to X_s\gamma$ is governed by the effective Hamiltonian at the b-quark mass scale $\mu=\mathcal{O}(m_b)$ [34,36],

$$\mathcal{H}_{\mathrm{Eff}}(b\to s\gamma) = -\frac{G_F}{\sqrt{2}}\lambda_{sb}^t\left[\sum_{i=1}^{6}C_i(\mu)O_i(\mu)+C_{7\gamma}(\mu)O_{7\gamma}(\mu)+C_{8G}(\mu)O_{8G}(\mu)\right], \tag{85}$$

where O_i and C_i $(i=1,\ldots,6)$ denote the four-Fermi operators and their Wilson coefficients, respectively. The effective operators $O_{7\gamma}$ and O_{8G} are given by

$$O_{7\gamma} = \frac{e}{8\pi^2}m_b\bar{s}\sigma_{\mu\nu}(1+\gamma_5)bF_A^{\mu\nu}, \tag{86}$$

$$O_{8G} = \frac{g_s}{8\pi^2}m_b\bar{s}\frac{\lambda^a}{2}\sigma_{\mu\nu}(1+\gamma_5)bG^{a\mu\nu}. \tag{87}$$

In the calculation of the branching ratio for $\bar{B}\to X_s\gamma$, it is convenient to introduce the so-called "effective coefficients" $C_i^{(0)\mathrm{eff}}$ [37,38]. The effective coefficient for the effective operator $O_{7\gamma}$ at the scale $\mu=\mathcal{O}(m_b)$ is given as [34,38,39]

$$C_{7\gamma}^{(0)\mathrm{eff}}(\mu) = \eta^{\frac{16}{23}}C_{7\gamma}^{(0)}(M_W)+\frac{8}{3}\left(\eta^{\frac{14}{23}}-\eta^{\frac{16}{23}}\right)C_{8G}^{(0)}(M_W)+C_2^{(0)}(M_W)\sum_{i=1}^{8}h_i\eta^{a_i}, \tag{88}$$

where $\eta = \alpha_s(M_W)/\alpha_s(\mu)$ with $\alpha_s = g_s^2/(4\pi)$ and

$$h_i = \left(2.2996,\ -1.0880,\ -\frac{3}{7},\ -\frac{1}{14},\ -0.6494,\ -0.0380,\ -0.0185,\ -0.0057\right), \tag{89}$$

$$a_i = \left(\frac{14}{23}, \frac{16}{23}, \frac{6}{23},\ -\frac{12}{23}, 0.4086,\ -0.4230,\ -0.8994, 0.1456\right). \tag{90}$$

In Eq. (88), the indices "(0)" mean the leading-order contributions. Since we do not take into account the running effect from the VLQ mass scale to the EW scale, we obtain the Wilson coefficients $C_{7\gamma}^{(0)}$ and $C_{8G}^{(0)}$ at the EW scale (taken as M_W) as:

$$C_{7\gamma}^{(0)}(M_W) = C_{7\gamma}^{\mathrm{SM}}(M_W) + C_{7\gamma}^{\mathrm{NP1}}(M_W) + C_{7\gamma}^{\mathrm{NP2}}(M_W), \tag{91}$$

$$C_{8G}^{(0)}(M_W) = C_{8G}^{\mathrm{SM}}(M_W) + C_{8G}^{\mathrm{NP1}}(M_W) + C_{8G}^{\mathrm{NP2}}(M_W), \tag{92}$$

where the Wilson coefficients,

$$C_{7\gamma}^{\mathrm{SM}}(M_W) = -\frac{1}{2}\left[Q_u F_u(x_t) + F_W(x_t)\right], \tag{93}$$

$$C_{8G}^{\mathrm{SM}}(M_W) = -\frac{1}{2} F_u(x_t), \tag{94}$$

come from the SM contributions in Eq. (52). The Wilson coefficients

$$C_{7\gamma}^{\mathrm{NP1}}(M_W) = C_{7\gamma}^{\mathrm{NP1}}(M_4) = \frac{Q_d}{24} \cdot \frac{Z_{\mathrm{NC}}^{sb}}{\lambda_{sb}^t}, \tag{95}$$

$$C_{8G}^{\mathrm{NP1}}(M_W) = C_{8G}^{\mathrm{NP1}}(M_4) = \frac{1}{24} \cdot \frac{Z_{\mathrm{NC}}^{sb}}{\lambda_{sb}^t}, \tag{96}$$

are obtained from the VLQ contributions in Eqs. (41) and (42). The Wilson coefficients $C_{7\gamma}^{\mathrm{NP2}}$ and C_{8G}^{NP2} are given as follows:

$$C_{7\gamma}^{\mathrm{NP2}}(M_W) = C_{7\gamma}^{\mathrm{uv}}(M_W) + C_{7\gamma}^{\mathrm{NC}}(M_W), \tag{97}$$

$$C_{8G}^{\mathrm{NP2}}(M_W) = C_{8G}^{\mathrm{uv}}(M_W) + C_{8G}^{\mathrm{NC}}(M_W), \tag{98}$$

where

$$\begin{aligned} C_{7\gamma}^{\mathrm{uv}}(M_W) &= \frac{1}{2}\left(\frac{2}{3}Q_u + \frac{5}{6}\right) \cdot \frac{Z_{\mathrm{NC}}^{sb}}{\lambda_{sb}^t}, \quad & C_{7\gamma}^{\mathrm{NC}}(M_W) &= \frac{Q_d}{3}\left(1 - Q_d s_w^2\right) \cdot \frac{Z_{\mathrm{NC}}^{sb}}{\lambda_{sb}^t}, \\ C_{8G}^{\mathrm{uv}}(M_W) &= \frac{1}{3} \cdot \frac{Z_{\mathrm{NC}}^{sb}}{\lambda_{sb}^t}, & C_{8G}^{\mathrm{NC}}(M_W) &= \frac{1}{3}\left(1 - Q_d s_w^2\right) \cdot \frac{Z_{\mathrm{NC}}^{sb}}{\lambda_{sb}^t}. \end{aligned} \tag{99}$$

The Wilson coefficients with the suffix "uv" come from the effective Lagrangian in Eq. (53), whose origin is the violation of CKM unitarity. The Wilson coefficients with the suffix "NC" are obtained from the effective Lagrangian in Eq. (54) by taking the limits $r_p \to 0$ and $w_p \to 0$. Here we neglect $\mathcal{O}(Z_{\mathrm{NC}}^2)$ terms. The Wilson coefficients C_{8G}^{uv} and C_{8G}^{NC} can be obtained from the effective Lagrangian corresponding to the $b \to sg$ diagrams.

In our numerical calculation, we use the NLO expression for the branching ratio $\mathrm{Br}[\bar{B} \to X_s\gamma]$ given as [40]

$$\mathrm{Br}[\bar{B} \to X_s\gamma] = \mathrm{Br}[\bar{B} \to X_c e\overline{\nu_e}]_{\mathrm{Exp}} \cdot R_{\mathrm{quark}}(\delta)\left(1 - \frac{\delta_{sl}^{NP}}{m_b^2} + \frac{\delta_{rad}^{NP}}{m_b^2}\right), \tag{100}$$

where δ_{sl}^{NP} and δ_{rad}^{NP} are non-perturbative corrections for the semi-leptonic and radiative $\bar{B}$ meson decay rates, respectively. The quantity R_{quark} at NLO is summarized in Ref. [40] as

$$R_{\mathrm{quark}}(\delta) = \frac{\Gamma[b \to X_s\gamma]^{E_\gamma > (1-\delta)E_\gamma^{\max}}}{\Gamma[b \to X_c e\overline{\nu_e}]} = \frac{\left|\lambda_{sb}^t\right|^2}{\left|V_{\mathrm{CKM}}^{cb}\right|^2}\frac{6\alpha_{em}}{\pi g(z)}F(z)\left\{|D|^2 + A(\delta)\right\}. \tag{101}$$

The function $g(z)$ with $z = m_{c,\mathrm{pole}}^2/m_{b,\mathrm{pole}}^2$ corresponds to the phase space factor for the semi-leptonic decay. The function $F(z)$ contains the NLO correction for the semi-leptonic decay and the difference between the pole mass and the $\overline{\mathrm{MS}}$ mass of the b-quark. The δ is the lower cut on the photon energy in the bremsstrahlung correction:

$$E_\gamma > (1-\delta)E_\gamma^{\max} \equiv (1-\delta)\frac{m_b}{2}. \tag{102}$$

The term $A(\delta)$ originates from the bremsstrahlung corrections and the virtual corrections [40–43],

$$A = \left\{e^{-\frac{\alpha_s(\mu_b)}{3\pi}(7+2\ln\delta)\ln\delta} - 1\right\}\left|C_{7\gamma}^{(0)\mathrm{eff}}(\mu_b)\right|^2 + \frac{\alpha_s(\mu_b)}{\pi}\sum_{\substack{i,j=1\\ i\le j}}^{8} C_i^{(0)\mathrm{eff}}(\mu_b)C_j^{(0)\mathrm{eff}}(\mu_b)f_{ij}(\delta), \tag{103}$$

where the functions $f_{ij}(\delta)$ can be found in Ref. [40]. The term $|D|^2$ in Eq. (101) is constituted by the NLO Wilson coefficient for $O_{7\gamma}$ and the virtual corrections for $b \to s\gamma$ [40–42]. Here, D is defined as

$$D = C_{7\gamma}^{(0)\mathrm{eff}}(\mu_b) + \frac{\alpha_s(\mu_b)}{4\pi}\left[C_{7\gamma}^{(1)\mathrm{eff}}(\mu_b) + \sum_{i=1}^{8} C_i^{(0)\mathrm{eff}}(\mu_b)\left\{r_i + \gamma_{i7}^{(0)\mathrm{eff}}\ln\frac{m_b}{\mu_b}\right\}\right], \tag{104}$$

where $C_{7\gamma}^{(1)\mathrm{eff}}(\mu_b)$, r_i, and $\gamma_{i7}^{(0)\mathrm{eff}}$ can be found in Ref. [40].

In our numerical calculation, we take $\mu_b = m_b$, $E_\gamma > 1.6$ GeV, and neglect the $\mathcal{O}(\alpha_s)$ correction to the new physics contributions. Therefore the Wilson coefficients $C_{7\gamma,8G}^{\mathrm{NP1}}$ and $C_{7\gamma,8G}^{\mathrm{NP2}}$ are only included in the first term in Eq. (104).

4.4. *Violation of CKM unitarity*

The violation of CKM unitarity is shown in Eq. (40). For $p = b, q = s$, we obtain the following relation:

$$\lambda_{bs}^u + \lambda_{bs}^c + \lambda_{bs}^t = Z_{\mathrm{NC}}^{bs}. \tag{105}$$

This relation can be rewritten as follows:

$$\left|\frac{\lambda_{bs}^c}{\lambda_{bs}^t}\right|^2\left(1 - 2\left|\frac{\lambda_{bs}^u}{\lambda_{bs}^c}\right|\cos\gamma_s + \left|\frac{\lambda_{bs}^u}{\lambda_{bs}^c}\right|^2\right) = 1 - 2r_{sb}\cos\theta_{sb} + r_{sb}^2, \tag{106}$$

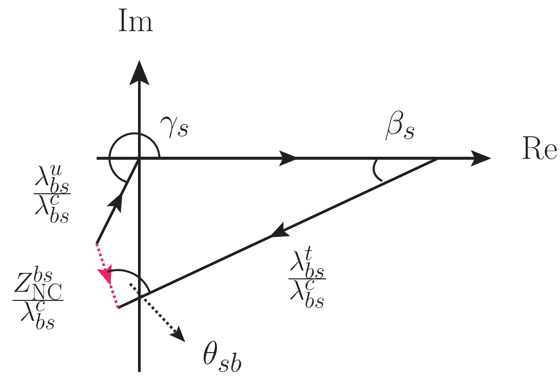

Fig. 7. The violation of CKM unitarity, Eq. (105), in the complex plane. We multiply the relation in Eq. (105) by a factor of $1/\lambda^c_{bs}$.

where we define

$$\gamma_s \equiv \arg\left[-\frac{\lambda^u_{bs}}{\lambda^c_{bs}}\right]. \tag{107}$$

The relation in Eq. (105) leads to a quadrilateral in the complex plane, as shown in Fig. 7.

4.5. Numerical analyses

In the following numerical analyses, we obtain constraints on FCNC couplings by using the current experimental data of rare B decays, $B_s \to \mu^+\mu^-$ and $\bar{B} \to X_s\gamma$. We also take account of the quadrilateral constraint Eq. (106) and Fig. 7. The values of the input parameters used in the numerical analyses are shown in Table 1.

At first we analyze the branching ratio of the $B_s \to \mu^+\mu^-$ process by using the expression in Eq. (83). Note that the branching ratio depends on the new physics parameters r_{sb} and $\cos\theta_{sb}$. We equate $\mathrm{Br}[B_s \to \mu^+\mu^-]_{\rm VLQ}$ in Eq. (83) with the experimental value,

$$\mathrm{Br}[B_s \to \mu^+\mu^-]_{\rm VLQ} = \mathrm{Br}[B_s \to \mu^+\mu^-]_{\rm Exp}. \tag{108}$$

As the experimental value, we adopt the branching ratio measured by LHCb [45]:

$$\mathrm{Br}[B_s \to \mu^+\mu^-]_{\rm Exp} = \left(3.0 \pm 0.6^{+0.3}_{-0.2}\right) \times 10^{-9}. \tag{109}$$

In Fig. 8, we show the dependence of $\mathrm{Br}[B_s \to \mu^+\mu^-]_{\rm VLQ}$ on the absolute value of the FCNC coupling $\left|Z^{sb}_{\rm NC}\right|$. The different colors of the dots in the scattered plots represent the different ranges for the value of the new physics parameter $|\theta_{sb}|$. The colored region satisfies the quadrangle constraint Eq. (106) with $0 \leq \gamma_s \leq 2\pi$. Note that the expression of the branching ratio and quadrilateral constraint depend on θ_{sb} through its cosine, and the plotted regions do not depend on the sign of θ_{sb}. The experimentally allowed range of the branching ratio in Eq. (109) is shown as the gray shaded region. The horizontal solid line corresponds to the central value of the experimental branching ratio in Eq. (109). In Fig. 8, as $\left|Z^{sb}_{\rm NC}\right|$ approaches zero, $\mathrm{Br}[B_s \to \mu^+\mu^-]_{\rm VLQ}$ comes close to the SM prediction [35],

$$\mathrm{Br}[B_s \to \mu^+\mu^-]_{\rm SM} = (3.23 \pm 0.27) \times 10^{-9}. \tag{110}$$

As $\left|Z^{sb}_{\rm NC}\right|$ increases from zero to 3×10^{-4}, $\mathrm{Br}[B_s \to \mu^+\mu^-]_{\rm VLQ}$ decreases for $|\theta_{sb}| < \pi/2$, while it increases for $\pi/2 < |\theta_{sb}| < \pi$. As $\left|Z^{sb}_{\rm NC}\right|$ becomes larger, $\mathrm{Br}[B_s \to \mu^+\mu^-]_{\rm VLQ}$ increases regardless

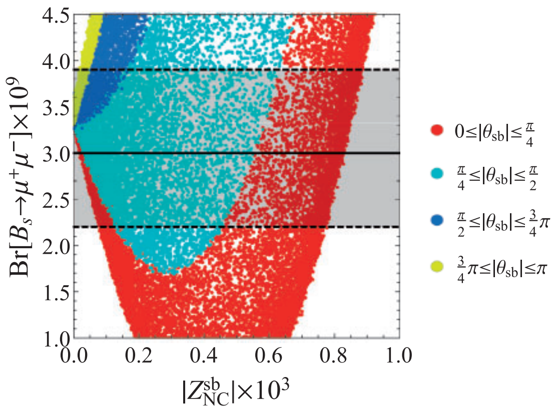

Fig. 8. The dependence of $\mathrm{Br}[B_s \to \mu^+\mu^-]_{\mathrm{VLQ}}$ on the FCNC coupling $\left|Z_{\mathrm{NC}}^{sb}\right|$. The different colors of the dots represent the different ranges for the value of $|\theta_{sb}|$. The colored region satisfies the quadrilaterl constraint Eq. (106) with $0 \leq \gamma_s \leq 2\pi$. The experimentally allowed range of the branching ratio in Eq. (109) is shown as the gray shaded region. The horizontal solid line corresponds to the central value of the experimental branching ratio in Eq. (109).

of the range of $|\theta_{sb}|$ since the third term in Eq. (84) is dominant. The dependence on $|\theta_{sb}|$ for smaller $\left|Z_{\mathrm{NC}}^{sb}\right|$ can be also understood from Eq. (84), since the coefficient of the term linear in r_{sb} is proportional to $\cos\theta_{sb}$.

Next we analyze the branching ratio of the $\bar{B} \to X_s\gamma$ process by using the expression in Eq. (100). Here we denote the branching ratio in the model with VLQ as $\mathrm{Br}[\bar{B} \to X_s\gamma]_{\mathrm{VLQ}}$. The new physics parameters r_{sb} and θ_{sb} are included in the Wilson coefficients in Eqs. (91) and (92). In order to obtain constraints on r_{sb} and θ_{sb}, we take account of the current average [46],

$$\mathrm{Br}[\bar{B} \to X_s\gamma]_{\mathrm{Exp}} = (3.32 \pm 0.15) \times 10^{-4}, \tag{111}$$

of experimental data [47–53]. In Fig. 9, we show the dependence of $\mathrm{Br}[\bar{B} \to X_s\gamma]_{\mathrm{VLQ}}$ on $|Z_{\mathrm{NC}}^{sb}|$. The different colors of the dots in the scattered plots represent the different ranges for the value of the new physics parameter $|\theta_{sb}|$. The colored region satisfies the quadrilateral constraint Eq. (106) with $0 \leq \gamma_s \leq 2\pi$. The experimentally allowed range of the branching ratio in Eq. (111) is shown as the gray shaded region. The horizontal solid line corresponds to the central value of the experimental branching ratio in Eq. (111). In Fig. 9, as $|Z_{\mathrm{NC}}|$ approaches zero, the value of $\mathrm{Br}[\bar{B} \to X_s\gamma]_{\mathrm{VLQ}}$ comes close to that of the SM prediction at NNLO accuracy [54],

$$\mathrm{Br}[\bar{B} \to X_s\gamma]_{\mathrm{SM}} = (3.36 \pm 0.23) \times 10^{-4}. \tag{112}$$

We note that the number of light-blue dots is much less than that of the red ones, since the quadrilateral constraint for $\pi/4 \leq \theta_{sb} \leq \pi/2$ is tighter than that for $0 \leq \theta_{sb} \leq \pi/4$. For the smaller $\left|Z_{\mathrm{NC}}^{sb}\right|$, the filled regions with colored dots are almost the same as each other. Thus, $\mathrm{Br}[B \to X_s\gamma]_{\mathrm{VLQ}}$ depends on $|\theta_{sb}|$ weakly compared with $\mathrm{Br}[B_s \to \mu^+\mu^-]_{\mathrm{VLQ}}$.

In the left figure of Fig. 10, we show the region allowed by the experimental data for the parameters r_{sb} and θ_{sb}. The blue dots satisfy both the constraint from $\mathrm{Br}[B_s \to \mu^+\mu^-]_{\mathrm{Exp}}$ and the quadrilateral constraint Eq. (106) with $0 \leq \gamma_s \leq 2\pi$. The green dots satisfy both the constraint from $\mathrm{Br}[\bar{B} \to X_s\gamma]_{\mathrm{Exp}}$ and the quadrilateral constraint. The values of r_{sb} and θ_{sb} in the region where the blue and green region overlap satisfy all three constraints. The blue region has the shape of a ring. The region inside the ring is excluded because r_{sb} and θ_{sb} in this region lead to predictions of $\mathrm{Br}[B_s \to \mu^+\mu^-]$

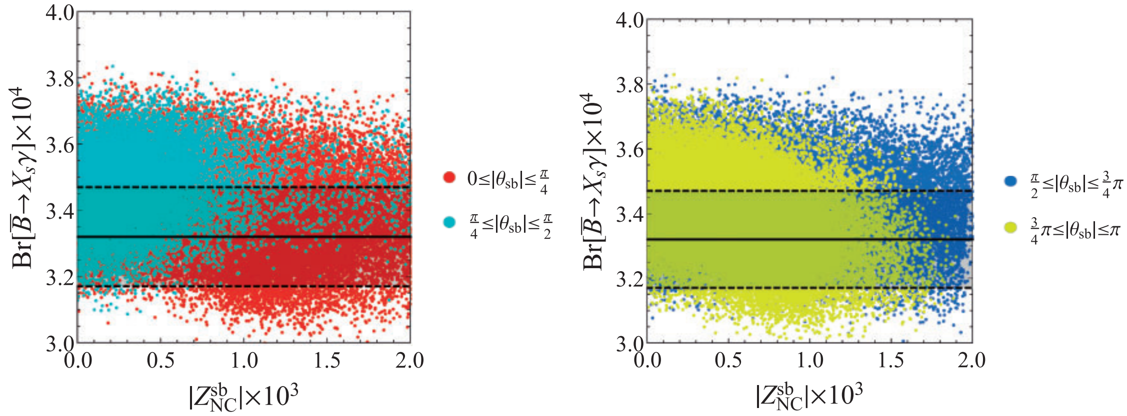

Fig. 9. The dependence of $\mathrm{Br}[\bar{B}\to X_s\gamma]_{\mathrm{VLQ}}$ on $|Z_{\mathrm{NC}}^{sb}|$. The different colors of the dots represent the different ranges for the value of $|\theta_{sb}|$. The colored region satisfies the quadrilateral constraint Eq. (106) with $0\le\gamma_s\le 2\pi$. The experimentally allowed range of the branching ratio in Eq. (111) is shown as the gray shaded region. The horizontal solid line corresponds to the central value of the experimental branching ratio in Eq. (111).

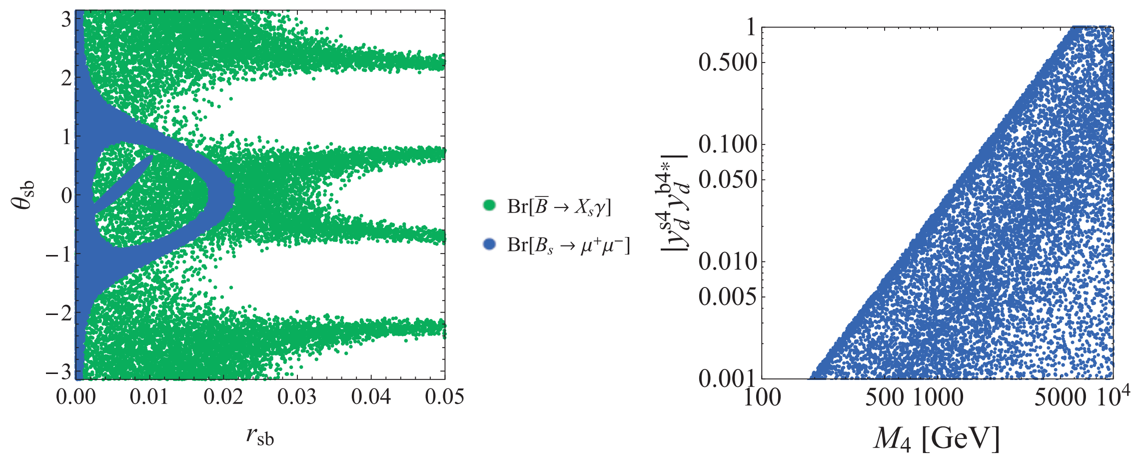

Fig. 10. (Left): The region allowed by the experimental data for the parameters r_{sb} and θ_{sb}. The blue dots satisfy both the constraint from $\mathrm{Br}[B_s\to\mu^+\mu^-]_{\mathrm{Exp}}$ and the quadrilateral constraint Eq. (106) with $0\le\gamma_s\le 2\pi$. The green dots satisfy both the constraint from $\mathrm{Br}[\bar{B}\to X_s\gamma]_{\mathrm{Exp}}$ and the quadrilateral constraint. (Right): The constraint on the VLQ mass M_4 and the product of the Yukawa coupling $|y_d^{s4}y_d^{b4*}|$. The blue region satisfies the constraints from $\mathrm{Br}[B_s\to\mu^+\mu^-]_{\mathrm{Exp}}$ and the quadrilateral constraint Eq. (106).

smaller than the experimental value. One finds that the stringent constraint on the parameters r_{sb} and θ_{sb} comes from $\mathrm{Br}[B_s\to\mu^+\mu^-]_{\mathrm{Exp}}$.

Using the definition of Z_{NC} in Eq. (39), we obtain a constraint on the VLQ mass M_4 and the product of the Yukawa coupling $|y_d^{s4}y_d^{b4*}|$. This result is shown in the right figure of Fig. 10, where we use $v = 246$ GeV [44]. Since the constraint on r_{sb} and θ_{sb} from $\mathrm{Br}[B_s\to\mu^+\mu^-]_{\mathrm{Exp}}$ is stronger than that from $\mathrm{Br}[\bar{B}\to X_s\gamma]_{\mathrm{Exp}}$ (see Fig. 10 left), we show the region with blue dots where $(M_4, |y_d^{s4}y_d^{b4*}|)$ satisfy the constraint from $\mathrm{Br}[B_s\to\mu^+\mu^-]_{\mathrm{Exp}}$ and the quadrilateral constraint Eq. (106). One finds that the lower limit on the VLQ mass is around 5.5 TeV for $\left|y_d^{s4}y_d^{b4*}\right|\sim 1$.

Finally, we show the violation of CKM unitarity on the complex plane in Fig. 11. The definition of each side is the same as that of Fig. 7. In order to obtain Fig. 11, we choose $r_{sb} = 0.018$ and $|\theta_{sb}| = \pi/6$ and use the central values of the CKM matrix elements in Table 1. The side for λ_{bs}^t is connected with the real axis at $(1, 0)$. The left figure is the case of $\theta_{sb} = \pi/6$, while the right figure

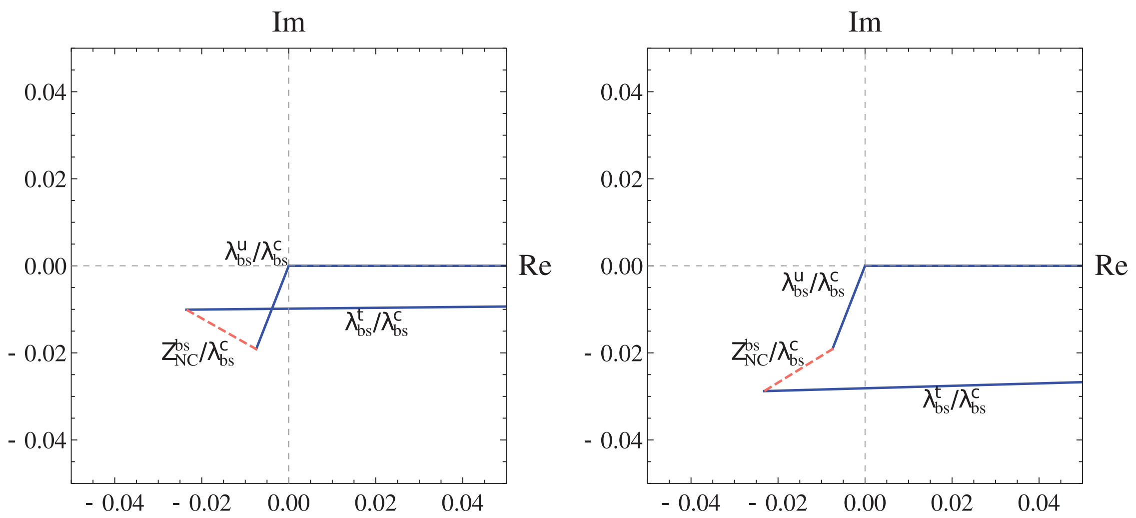

Fig. 11. The violation of CKM unitarity on the complex plane. In order to obtain these figures, we choose $(r_{sb}, \theta_{sb}) = (0.018, \pi/6)$ in the left figure and $(r_{sb}, \theta_{sb}) = (0.018, -\pi/6)$ in the right figure.

is that of $\theta_{sb} = -\pi/6$. One can see that the side for $Z_{\rm NC}^{sb}$ can be as large as that for λ_{bs}^{u}, and the sign of θ_{sb} affects the value of the angle β_s in Fig. 7.

5. Summary and discussion

We have studied the model that includes one down-type SU(2) singlet VLQ in addition to the SM quarks and shown the constraints on the model parameters from $\mathrm{Br}[B_s \to \mu^+\mu^-]$, $\mathrm{Br}[\bar{B} \to X_s\gamma]$, and the quadrilateral relation. In order to analyze this model, we used the effective theory derived by integrating out the VLQ field. We assume that the mass of the VLQ is much larger than the EW scale. We matched the effective theory with the full theory not only at tree level but also at one-loop level, and obtained the effective operators related to the radiative transition of the quarks. These operators correspond to the contribution from the diagrams including the VLQ in the internal line. One can find that the coefficient of the photon dipole operator with the down-type quarks is consistent with the case of the full theory calculation given in Ref. [25].

The other contributions to the radiative transitions come from the violation of CKM unitarity and the diagrams that include the FCNC couplings among the SM quarks. We obtained the effective Lagrangian for the $b \to s\gamma^{(*)}$ process arising from these contributions.

From our numerical results, we obtained the constraints on the FCNC coupling $Z_{\rm NC}^{sb}$ and the new physics parameters (r_{sb}, θ_{sb}) defined in Eq. (80). We found that the dependence of $\mathrm{Br}[\bar{B} \to X_s\gamma]_{\rm VLQ}$ on θ_{sb} is weaker than that of $\mathrm{Br}[B_s \to \mu^+\mu^-]_{\rm VLQ}$, and the constraint on the model parameters r_{sb} and θ_{sb} from $\mathrm{Br}[B_s \to \mu^+\mu^-]$ is more stringent than that from $\mathrm{Br}[\bar{B} \to X_s\gamma]$. One can discriminate the cases of different $|\theta_{sb}|$ through $\mathrm{Br}[B_s \to \mu^+\mu^-]$, as shown in Fig. 8. When $|Z_{\rm NC}^{sb}|$ is of the order of 10^{-4}, $\mathrm{Br}[B_s \to \mu^+\mu^-]$ becomes small (large) for $|\theta_{sb}| \simeq 0$ ($|\theta_{sb}| \simeq \pi$) compared with that of the SM. In Fig. 11, we showed the violation of CKM unitarity on the complex plane when we chose $r_{sb} = 0.018$ and $|\theta_{sb}| = \pi/6$. The difference in the sign of θ_{sb} affects the angle β_s, therefore we have to investigate the constraint from the observables related to β_s to further restrict the form of the violation of CKM unitarity.

Although we focused on the case of $b \to s$ transitions, the effective Lagrangian obtained in this paper can be applied to the FCNC transition for other combinations of the down-type quarks.

The four-Fermi operators in Eqs. (9)–(11) and the effective Lagrangian for the off-shell photon contribute to $b \to sl^+l^-$ processes, including $\bar{B} \to \bar{K}^* l^+ l^-$.

Finally, we add a comment on the renormalization group effect. One cannot neglect the effect when the VLQ mass is much heavier than the EW scale. When $M_4/M_W \sim 100$, one may expect about 10% corrections to the Wilson coefficients. Moreover, the expressions for the FCNC coupling, CKM matrix elements, and down-type quark masses will be modified. Including them, we will carry out the precise analysis elsewhere.

Acknowledgements

This work is supported by JSPS KAKENHI Grant Numbers JP16H03993 and JP17K05418 (T.M.). This work is also supported in part by Grants-in-Aid for Scientific Research [Nos. 16J05332 (Y.S.), 24540272, 26247038, 15H01037, 16H00871, and 16H02189 (H.U.)] from the Ministry of Education, Culture, Sports, Science and Technology in Japan.

Funding

Open Access funding: SCOAP^3.

References

[1] S. L. Glashow, J. Iliopoulos, and L. Maiani, Phys. Rev. D **2**, 1285 (1970).
[2] M. Kobayashi and T. Maskawa, Prog. Theor. Phys. **49**, 652 (1973).
[3] N. Cabibbo, Phys. Rev. Lett. **10**, 531 (1963).
[4] M. Gell-Mann and M. Lévy, Nuovo Cim. **16**, 705 (1960).
[5] J. Charles et al. [CKMfitter Group], Eur. Phys. J. C **41**, 1 (2005) [arXiv:hep-ph/0406184] [Search INSPIRE].
[6] M. Bona et al. [UTfit Collaboration], J. High Energy Phys. **03**, 049 (2008) [arXiv:0707.0636 [hep-ph]] [Search INSPIRE].
[7] Z. G. Berezhiani, Phys. Lett. B **129**, 99 (1983).
[8] Z. G. Berezhiani, Phys. Lett. B **150**, 177 (1985).
[9] S. Rajpoot, Phys. Lett. B **191**, 122 (1987).
[10] S. Rajpoot, Phys. Rev. D **36**, 1479 (1987).
[11] A. Davidson and K. C. Wali, Phys. Rev. Lett. **59**, 393 (1987).
[12] Z. G. Berezhiani and R. Rattazzi, Phys. Lett. B **279**, 124 (1992).
[13] K. S. Babu and R. N. Mohapatra, Phys. Rev. D **41**, 1286 (1990).
[14] G. Barenboim, F. J. Botella, and O. Vives, Nucl. Phys. B **613**, 285 (2001) [arXiv:hep-ph/0105306] [Search INSPIRE].
[15] F. J. Botella, G. C. Branco, and M. Nebot, J. High Energy Phys. **12**, 040 (2012) [arXiv:1207.4440 [hep-ph]] [Search INSPIRE].
[16] A. K. Alok, S. Banerjee, D. Kumar, and S. Uma Sankar, Nucl. Phys. B **906**, 321 (2016) [arXiv:1402.1023 [hep-ph]] [Search INSPIRE].
[17] A. K. Alok, S. Banerjee, D. Kumar, S. U. Sankar, and D. London, Phys. Rev. D **92**, 013002 (2015) [arXiv:1504.00517 [hep-ph]] [Search INSPIRE].
[18] K. Ishiwata, Z. Ligeti, and M. B. Wise, J. High Energy Phys. **10**, 027 (2015) [arXiv:1506.03484 [hep-ph]] [Search INSPIRE].
[19] C. Bobeth, A. J. Buras, A. Celis, and M. Jung, J. High Energy Phys. **04**, 079 (2017) [arXiv:1609.04783 [hep-ph]] [Search INSPIRE].
[20] G. Aad et al. [The ATLAS Collaboration], J. High Energy Phys. **08**, 105 (2015) [arXiv:1505.04306 [hep-ex]] [Search INSPIRE].
[21] A. M. Sirunyan et al. [CMS Collaboration], arXiv:1708.02510 [hep-ex] [Search INSPIRE].
[22] F. del Aguila, M. Pérez-Victoria, and J. Santiago, Phys. Lett. B **492**, 98 (2000) [arXiv:hep-ph/0007160] [Search INSPIRE].
[23] F. del Aguila, J. Santiago, and M. Pérez-Victoria, J. High Energy Phys. **09**, 011 (2000) [arXiv:hep-ph/0007316] [Search INSPIRE].

[24] C. Y. Chen, S. Dawson, and E. Furlan, Phys. Rev. D **96**, 015006 (2017) [arXiv:1703.06134 [hep-ph]] [Search INSPIRE].

[25] L. T. Handoko and T. Morozumi, Mod. Phys. Lett. A **10**, 309 (1995); **10**, 1733 (1995) [erratum] [arXiv:hep-ph/9409240] [Search INSPIRE].

[26] T. Inami and C. S. Lim, Prog. Theor. Phys. **65**, 297 (1981); **65** (1981) 1772 [erratum].

[27] G. Buchalla, A. J. Buras, and M. K. Harlander, Nucl. Phys. B **349**, 1 (1991).

[28] G. C. Branco, T. Morozumi, P. A. Parada, and M. N. Rebelo, Phys. Rev. D **48**, 1167 (1993).

[29] G. C. Branco, P. A. Parada, T. Morozumi, and M. N. Rebelo, Phys. Lett. B **306**, 398 (1993).

[30] G. C. Branco, P. A. Parada, T. Morozumi, and M. N. Rebelo, Nucl. Phys. Proc. Suppl. A **37**, 29 (1994).

[31] G. Barenboim and F. J. Botella, Phys. Lett. B **433**, 385 (1998) [arXiv:hep-ph/9708209] [Search INSPIRE].

[32] C.-H. V. Chang, D. Chang, and W.-Y. Keung, Phys. Rev. D **61**, 053007 (2000) [arXiv:hep-ph/9811354] [Search INSPIRE].

[33] K.-i. Aoki, Z. Hioki, R. Kawabe, M. Konuma, and T. Muta, Prog. Theor. Phys. Suppl. **73**, 1 (1982).

[34] G. Buchalla, A. J. Buras, and M. E. Lautenbacher, Rev. Mod. Phys. **68**, 1125 (1996) [arXiv:hep-ph/9512380] [Search INSPIRE].

[35] A. J. Buras, J. Girrbach, D. Guadagnoli, and G. Isidori, Eur. Phys. J. C **72**, 2172 (2012) [arXiv:1208.0934 [hep-ph]] [Search INSPIRE].

[36] B. Grinstein, R. Springer, and M. B. Wise, Nucl. Phys. B **339**, 269 (1990).

[37] M. Ciuchini, E. Franco, G. Martinelli, L. Reina, and L. Silvestrini, Phys. Lett. B **316**, 127 (1993) [arXiv:hep-ph/9307364] [Search INSPIRE].

[38] A. J. Buras, M. Misiak, M. Münz, and S. Pokorski, Nucl. Phys. B **424**, 374 (1994) [arXiv:hep-ph/9311345] [Search INSPIRE].

[39] A. J. Buras, arXiv:hep-ph/9806471 [Search INSPIRE].

[40] K. Chetyrkin, M. Misiak, and M. Münz, Phys. Lett. B **400**, 206 (1997); **425** (1998) 414 [erratum] [arXiv:hep-ph/9612313] [Search INSPIRE].

[41] A. Ali and C. Greub, Phys. Lett. B **361**, 146 (1995) [arXiv:hep-ph/9506374] [Search INSPIRE].

[42] C. Greub, T. Hurth, and D. Wyler, Phys. Rev. D **54**, 3350 (1996) [arXiv:hep-ph/9603404] [Search INSPIRE].

[43] N. Pott, Phys. Rev. D **54**, 938 (1996) [arXiv:hep-ph/9512252] [Search INSPIRE].

[44] C. Patrignani et al. [Particle Data Group], Chin. Phys. C **40**, 100001 (2016).

[45] R. Aaij et al. [LHCb Collaboration], Phys. Rev. Lett. **118**, 191801 (2017) [arXiv:1703.05747 [hep-ex]] [Search INSPIRE].

[46] Y. Amhis et al. [Heavy Flavor Averaging Group], Eur. Phys. J. C **77**, 895 (2017) [arXiv:1612.07233 [hep-ex]] [Search INSPIRE].

[47] B. Aubert et al. [BaBar Collaboration], Phys. Rev. D **77**, 051103 (2008) [arXiv:0711.4889 [hep-ex]] [Search INSPIRE].

[48] J. P. Lees et al. [BaBar Collaboration], Phys. Rev. Lett. **109**, 191801 (2012) [arXiv:1207.2690 [hep-ex]] [Search INSPIRE].

[49] J. P. Lees et al. [BaBar Collaboration], Phys. Rev. D **86**, 052012 (2012) [arXiv:1207.2520 [hep-ex]] [Search INSPIRE].

[50] A. Limosani et al. [Belle Collaboration], Phys. Rev. Lett. **103**, 241801 (2009) [arXiv:0907.1384 [hep-ex]] [Search INSPIRE].

[51] T. Saito et al. [Belle Collaboration], Phys. Rev. D **91**, 052004 (2015) [arXiv:1411.7198 [hep-ex]] [Search INSPIRE].

[52] A. Abdesselam et al. [Belle Collaboration], arXiv:1608.02344 [hep-ex] [Search INSPIRE].

[53] S. Chen et al. [CLEO Collaboration], Phys. Rev. Lett. **87**, 251807 (2001) [arXiv:hep-ex/0108032] [Search INSPIRE].

[54] M. Misiak et al., Phys. Rev. Lett. **114**, 221801 (2015) [arXiv:1503.01789 [hep-ph]] [Search INSPIRE].